Project**: SEAWave**

Model validation and limitations for estimating occupational exposure

Work Package: WP2

Deliverable: D2.4

Deliverable No.: D8

Abstract

The systematic validation of the exposure scenarios outlined in Deliverable 2.2 is presented in this report. Employing standardized procedures, the validation analysis compares these scenarios with the in-situ RF-EMF measurement data detailed in Deliverable 2.3. The empirical data was collected from a range of environments, including private 5G networks—operating in both standalone (SA) and non-standalone (NSA) modes across the 3.5 GHz (FR1) and 26 GHz (FR2) bands—including Wi-Fi 6 equipment. These were deployed across diverse smart industrial and R&D settings, such as production facilities, warehousing, logistics operations, office spaces, and research sites.

Both the numerical tools and the generic model demonstrated good overall performance in estimating EMF exposure levels across diverse environments. The numerical simulations reliably reproduced general exposure characteristics as well as point-specific e-field estimation provided that the antennas and environments were modeled in sufficient detail. Similarly, the generic model showed strong agreement with measurements and simulations for median and 95th percentile values, confirming its capability to approximate realistic exposure conditions. Some deviations were observed in cases with atypical configurations or limited training data, suggesting that further refinement of the model through broader datasets could enhance its accuracy and generalization.

Project Details

Project name	SEAWave
Grant number	101057622
Start Date	01 Jun 2022
Duration	42 months
Scientific coordinator	Prof. Samaras T, Aristotle University of Thessaloniki (AUTH)

Deliverable Details

Deliverable related number	D2.4
Deliverable No.	D8
Deliverable name	Model validation and limitations for estimating occupational exposure

Work Package number	WP2
Work Package name	Occupational Exposures from New 5G Local Networks in Workplaces
Authors	Gajšek P, Apostolidis C, Trček T, Plets D, Valič B
Distribution	Public
Version	1.0
Draft/final	Final
Keywords	Validation, EMF exposure, Private networks

Contents

1 Introduction

In the critical field of EMF exposure assessment, the rigorous validation of computational simulations with precise empirical measurements is an indispensable practice for ensuring scientific credibility and public health protection. Simulations provide a powerful tool for modeling electromagnetic field (EMF) distribution in complex environments, predicting exposure levels from sources like base stations, and for evaluating exposure patterns, compliance with safety limits in various exposure scenarios.

However, these models rely on simplifications of geometry, material properties, and emission characteristics that may not fully capture reality. Empirical measurements, conducted with calibrated measuring equipment in controlled laboratory settings or real-world environments, serve as the essential ground truth, verifying the accuracy of simulations, identifying unmodeled propagation effects, and calibrating model parameters. This synergy is fundamental for building reliable, trustworthy assessment tools, which in turn form the basis for credible safety standards, defensible regulatory decisions, and ultimately, robust public confidence in the technologies that define our modern, connected world.

Validating theoretical Electromagnetic Field (EMF) models against empirical data is essential for bridging the gap between computational simulation and real-world exposure assessment. **Ray tracing methods** have been rigorously explored and validated for Radiofrequency (RF) EMF calculations in 5G base station networks, demonstrating reliability in predicting both spatial and temporal exposure patterns.

Up to date studies leveraging ray tracing frameworks incorporated detailed 3D environmental models (including building geometry, material properties, and multipath propagation) to simulate RF EMF distributions, particularly in dense working areas. Validation against empirical measurements of power density and electric field strength near 5G Massive Multiple-Input Multiple-Output (Massive MIMO) antennas with beamforming capabilities showed strong alignment, with discrepancies typically under 10% in far-field regions. Near-field scenarios, however, required finer mesh resolution to accurately account for beamforming edge effects [1, 2].

Hybrid methodologies, which combine ray tracing with FDTD techniques, have further improved accuracy in modeling localized exposure hotspots [3]. This approach is particularly beneficial in complex settings, such as industrial indoor environments with metallic obstructions. While challenges persist in capturing dynamic beamforming variations, advancements like the use of beam pattern envelopes and power reduction factors (e.g., a 0.25 scaling for time-averaged 5G traffic beams) have enhanced prediction accuracy [2]. These validated models offer a cost-effective alternative to continuous, operator-dependent measurements for compliance assessment [4, 5, 6].

Empirical and simulated findings consistently demonstrate that RF EMF levels, even during maximum network load, remain well below international safety limits established by ICNIRP.

Massive MIMO Exposure: Investigations of Massive MIMO downlink (DL) exposure at 3.5 GHz using Maximum Ratio Transmission precoding showed that the majority of exposure is concentrated in the vicinity of the User Equipment (UE), with a ≈10 dB enhancement of the time-averaged Poynting vector observed at the receiver location [1]. Crucially, it was found that the peak spatial-averaged Specific Absorption Rate (SAR) in 10 g in a phantom's head was directly proportional to the hot-spot power flux density and complied with ICNIRP basic restrictions.

User vs. Non-User Exposure: A specialized hybrid approach (ray tracing/FDTD) for assessing peak spatial-averaged SAR in 10 g due to a Massive MIMO array at 3.5 GHz revealed that the exposure experienced by users is nearly eight times higher than that of non-users [3].

Small Cell Base Stations (BS): Exposure assessments for widely deployed 5G small cell BS showed that levels were below occupational exposure limits (maximum exposure ratio of 0.15) at distances between 0.5 m and 1 m [6]. The exposure of a non-user within an active network is highly dependent on the distribution and usage patterns of users and the beamforming capabilities of the base station [5].

2 Validation methodology and criteria

To assess the reliability of the numerical models used in our simulations, their results are validated against measurements conduct in real environments with operational wireless local networks. Two approaches are applied: point-to-point comparison and overall exposure-characterization comparison. In both approaches, calculated and measured exposure metrics are compared while considering the uncertainty of the applied method.

For this purpose of validation, raster measurements were used, as they are equally distributed inside the area of interest and therefore give the best estimate for both 95th percentile and median value, values, which are most representative when describing the exposure.

For calculations, statistical values were calculated for two set of results: calculated values on the same locations as measurements and all set of calculated results, which is usually very high, as raster calculations were mostly performed on a 0.1×0.1 m grid, whereas raster measurements were mostly performed on a 10×10 m grid. Errors and Pearson correlation was not calculated for all set of calculated results, as this is not possible due to different size of sample compared to measurements. By including also, the comparison of the full set, additional information was achieved about the representativeness of the selected measurement locations for the exposures for the whole area analyzed.

2.1 Point to point comparison

The most direct method of validation is a point-to-point comparison between simulated and measured electric-field strengths. In this approach, the electric field estimated by the numerical model at each location is directly compared with the corresponding electric field measured during the measurement campaign. With this procedure, the model's ability to reproduce spatial variations of the electric field throughout the test environment is evaluated.

To quantify a possible agreement between simulated and measured electric-field values, their difference is calculated for each measurement point:

$$Diff_{point} = E_{meas,point} - E_{sim,point}$$

The combined measurement and simulation standard uncertainty is also determined for each point:

$$u_{c,point} = \sqrt{u_{meas}^2 + u_{sim,point}^2}$$

These two quantities are compared for every point. If the condition

$$|Diff_{point}| < u_{c,point}$$

is satisfied with 68% of the evaluation points, then the model is considered validated [7]. If the simulation uncertainty $u_{sim,point}$ cannot be determined the expanded measurement uncertainty $U_{meas,point}$ can be used in calculating the acceptance criterion.

Besides also Pearson correlation coefficient r was determined for the correlation between the measured and calculated values, the higher the number of the r parameter, the better the correlation of the calculated data with the measured data. The Pearson correlation coefficient was calculated for the square of the electric field.

2.2 General Exposure-Characterization Comparison

Point-to-point comparison of the electric field is the most stringent and rigorous method for validating the numerical models. However, in complex indoor environments many variables influence the detailed electric-field distribution that cannot be fully represented in the model (e.g., the precise locations and orientations of transmitters, the exact positions of clutter and measurement points etc.). These factors can lead to significant discrepancies between calculated and measured values in a point-by-point comparison, even when the overall exposure levels are very similar.

For this reason, a complementary validation approach is adopted that focuses on the overall distribution of exposure levels rather than on individual measurement points. This method evaluates whether the simulations successfully reproduce the broader exposure characteristics observed in the real environment.

Initially, a Kolmogorov–Smirnov (K-S) test is performed to assess the null hypothesis that the simulated and measured datasets originate from the same underlying distribution. If the K–S test rejects the null hypothesis, we conclude that the distributions are significantly different, and the validation of the model is considered failed. If not, the comparison proceeds by examining key descriptive statistics of the two datasets. Specifically, the 50th (median) and 95th percentiles of the electric-field strength are derived for both the simulated and measured data. These two values were selected because they effectively describe both the typical exposure conditions and the higher exposure levels that occur in localized regions within the measurement area.

For validation we use the E_n score, a statistic conventionally applied for proficiency testing in calibration and inter-laboratory comparison measurements [8]:

$$E_n = \frac{x_{sim} - x_{meas}}{\sqrt{U^2(x_{sim}) + U^2(x_{meas})}}$$

where x_{sim} is the percentile derived from the simulations ($x_{sim,50}$and $x_{sim,95}$) and x_{meas} is the corresponding percentile derived from the measurements. $U(x_{sim})$ and $U(x_{meas})$ are the expanded uncertainties of the percentiles' values.

The numerical model is considered validated under this approach if, for both percentiles, the following condition is satisfied:

$$-1 \leq E_n \leq 1$$

Since percentiles are not derived from closed-form mathematical expressions, their uncertainty can't be obtained from measurement or simulation uncertainty using the standard uncertainty

propagation method. Instead, we estimate the uncertainty of each percentile with the bootstrap method [9]. This involves repeatedly creating resampled datasets by drawing data points with replacement from the original measurement or simulation dataset, so a given datapoint may be selected multiple times or not at all.

Typically, about 1,000 such resamples are generated. The percentile under consideration is computed for each resample, producing an empirical distribution of that percentile. Assuming this distribution is approximately normal, the standard uncertainty, u(x), is taken as the standard deviation of the bootstrap percentile values. The expanded uncertainty, *U(x)*, can then be calculated as

$$U(x) = 1.96 \cdot u(x)$$

3 Validation of various exposure scenarios

3.1 Scenario 1: Smart Industry 4.0: Warehouse, private SA 5G FR1

In the warehouse, designed for the storage of materials and finished products, a private 5G network was installed. There are 4 small cell access points mounted on the ceiling and operating in the range 3700–3800 MHz with a maximum output power of 1 W. Details about the setup are given in deliverable D 2.2.

Results obtained by measurements and by numerical calculations are given in Table 1.

Table 1. Results of measurements and numerical calculations with comparison to measurement values. For calculations, values are given for two datasets: same 40 points as measurements (40 points) or all calculated points at the height of 1.5 m (all).

	measurements	MATLAB 1 40 points	NARDA 40 points	MATLAB 1 all	NARDA all
number of samples	40	40	40	32628	208328
maximum value [V/m]	1.41	1.14	1.26	1.47	1.45
95th percentile [V/m] E95	**1.01**	**0.85**	**0.98**	**0.90**	**1.06**
75th percentile [V/m]	0.60	0.50	0.60	0.40	0.50
mean value [V/m]	0.55	0.43	0.51	0.38	0.50
median value [V/m] E50	**0.39**	**0.20**	**0.37**	**0.15**	**0.34**
25th percentile [V/m]	0.24	0.07	0.26	0.02	0.23
standard deviation [V/m]	0.64	0.55	0.58	0.52	0.60
quartile coefficient of dispersion	0.43	0.74	0.39	0.88	0.38
root mean square error [v/m]		0.23	0.51		
normalized root mean square error		0.42	0.94		
Pearson correlation coefficient r		0.84	0.90		
Pearson correlation coefficient p		0.00	0.00		
Kolmogorov-Smirnov (K-S) test D-stat		0.38	0.10	0.43	0.14
Kolmogorov-Smirnov (K-S) test D-crit 0.05		0.30	0.30	0.21	0.21

From the results it is evident there is a good correlation between the measurements and results of models, as the r-value is 0.84 or higher and p value is below 0.05. Results for 95th percentile, 75th percentile and mean value agree well, but there is significant difference in 25th percentile, where results of numerical calculations of one model give significantly lower values. This is visible also from the scatter plot in Figure 2 where lower values points lay predominantly below ideal line for MATLAB 1 results. The reason is in the difference between the Narda EFC-400 and MATLAB tools how each handles transmission through pallet racks. The Narda tool applies a uniform attenuation value of 3 dB for the racks, which was selected through a parametric study to best match measured data. In contrast, the MATLAB model does not account for field transmission through objects, so the electric field can only propagate through the empty spaces within the racks, resulting in effective attenuation of up to 20 dB. This substantial difference is likely the main reason for the discrepancies observed between the two sets of simulation results.

Despite these limitations, both models demonstrated good agreement with measurements in terms of maximum, average, and 95th percentile values, with differences typically below 20%, as shown in Table 1.

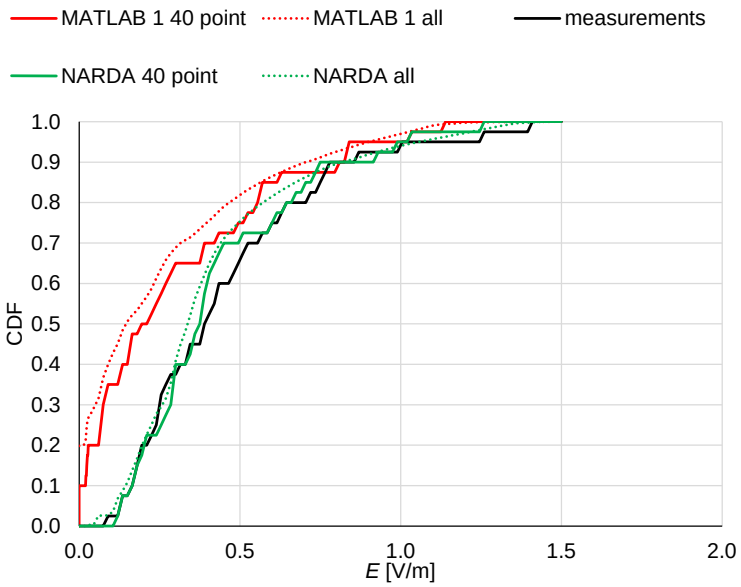

Figure 1. Cumulative distribution of measurements and calculations.

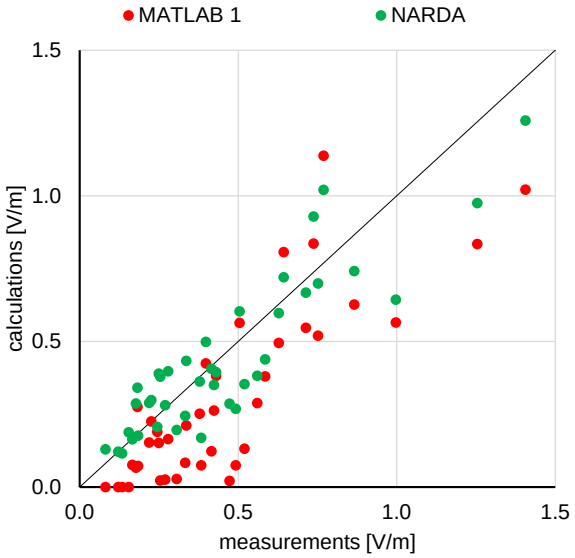

Figure 2. Scatter plots of measured values (x axis) and calculated values (y axis).

Kolmogorov-Smirnov test and cumulative distribution plot in Figure 1 for all calculation points showed good agreement between calculated results on 40 points and all calculated results,

meaning measurements and calculations on selected 40 points represent well the distribution of the electric field on the whole analyzed area. The same observation, that MATLAB 1 model gives lower values compared to measurements and NARDA model at areas with lower coverage is also visible from the cumulative distribution plot in Figure 1, as the cumulative distribution for MATLAB 1 lies slightly to the left at lower CDF values and realign with other results at higher values. For this case, the value of the Kolmogorov-Smirnov test surpassed the critical value for the 95% confidence interval.

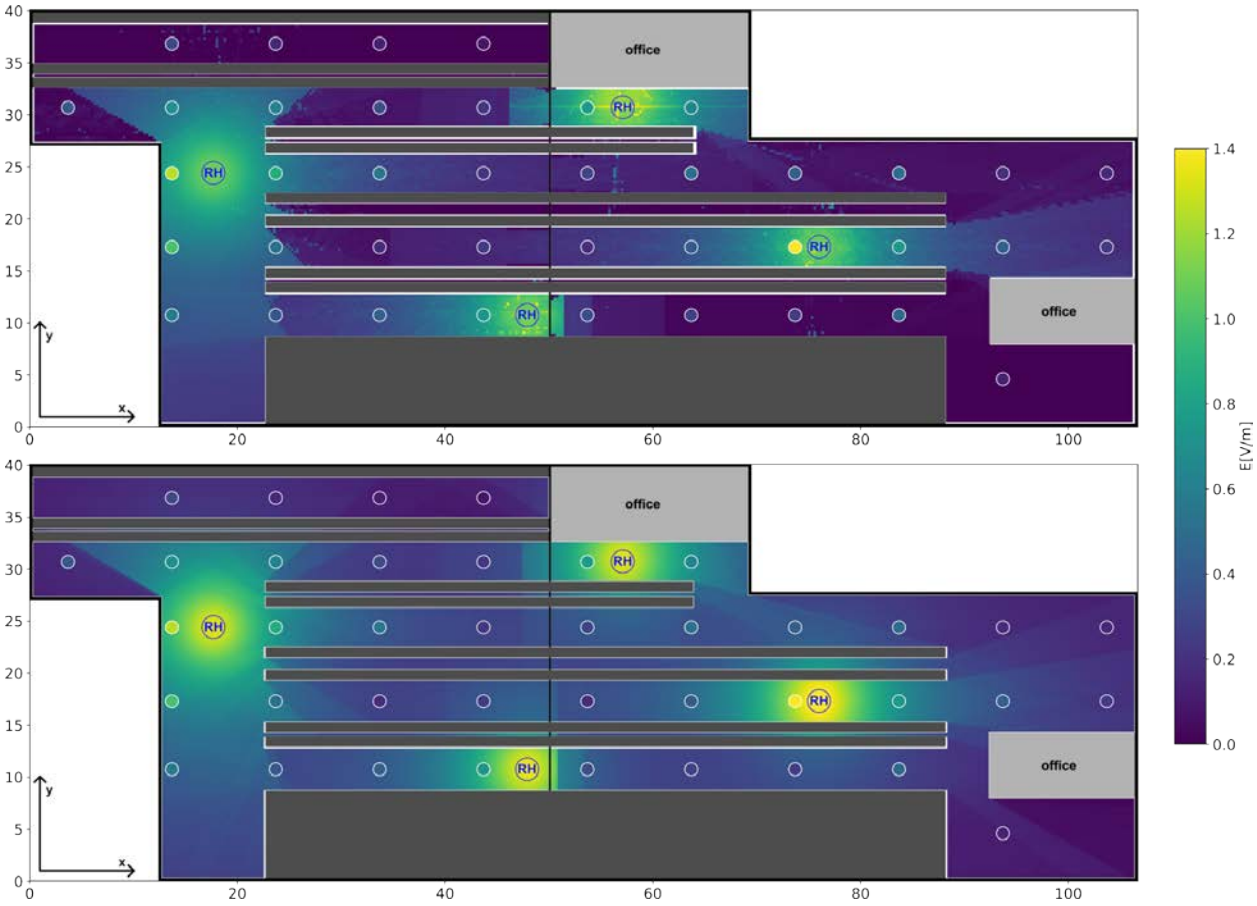

Figure 3. Results of calculations (colored layer) and measurements (dots with white border). From top to bottom: MATLAB 1 model and NARDA model.

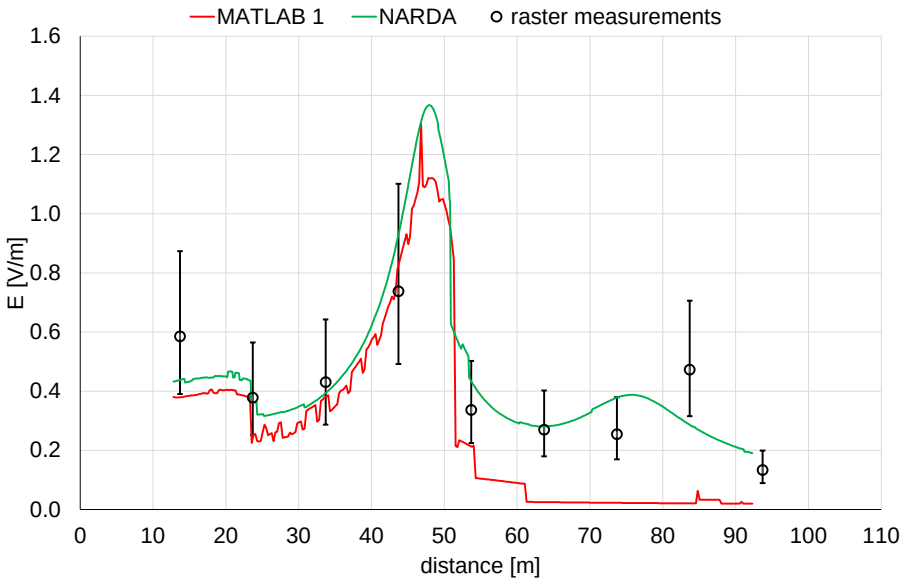

Figure 4: Electric field values along corridor 1. The results are given for the extrapolated maximum value. Circles represent the values measured during raster measurements together with measurement uncertainty. The distance is the distance along the corridor starting at the very left end of the Figure 3.

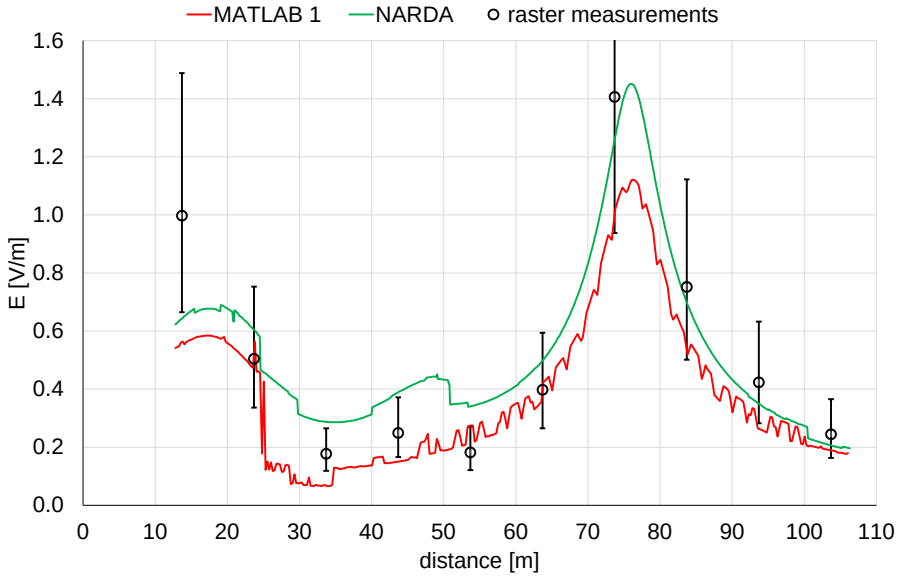

Figure 5. Electric field values along corridor 2. The results are given for the extrapolated maximum value. Circles represent the values measured during raster measurements together with measurement uncertainty. The distance is the distance along the corridor starting at the very left end of the Figure 3.

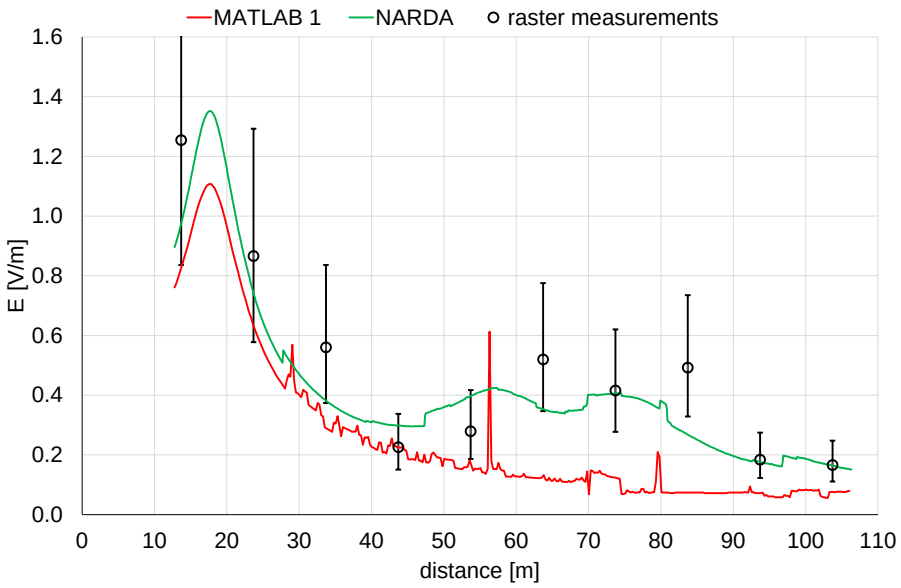

Figure 6. Electric field values along corridor 3. The results are given for the extrapolated maximum value. Circles represent the values measured during raster measurements together with measurement uncertainty. The distance is the distance along the corridor starting at the very left end of the Figure 3.

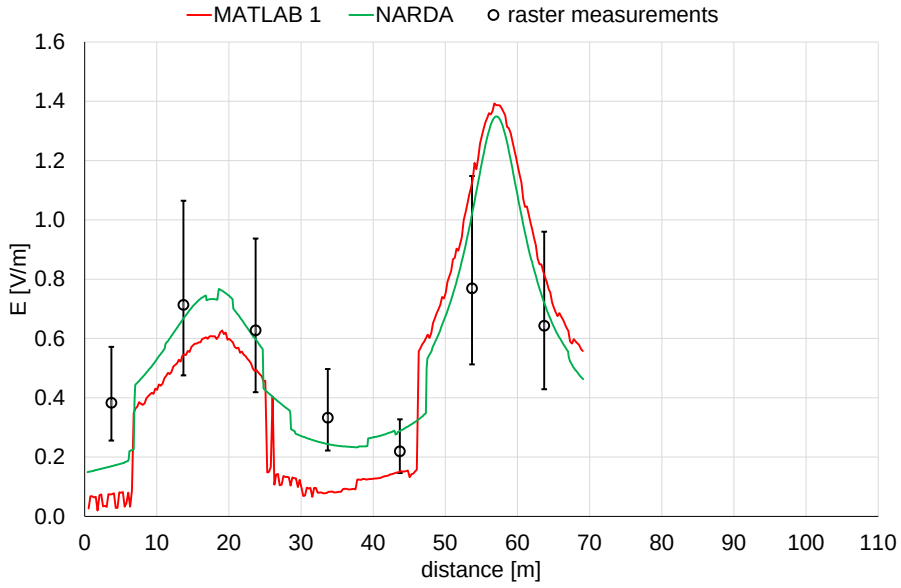

Figure 7. Electric field values along corridor 4. The results are given for the extrapolated maximum value. Circles represent the values measured during raster measurements together with measurement uncertainty. The distance is the distance along the corridor starting at the very left end of the Figure 3.

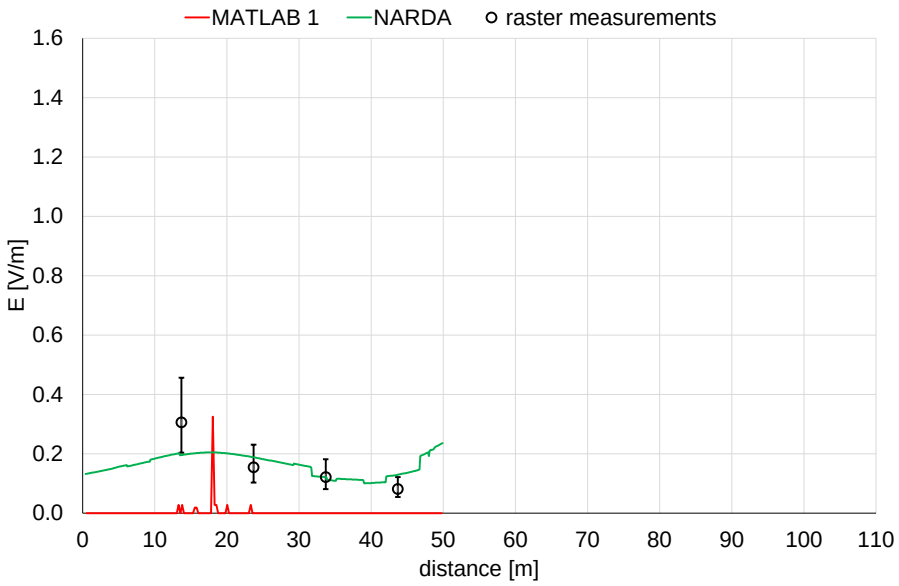

Figure 8. Electric field values along corridor 5. The results are given for the extrapolated maximum value. Circles represent the values measured during raster measurements together with measurement uncertainty. The distance is the distance along the corridor starting at the very left end of the Figure 3.

From the comparisons of results of measurements and calculations along the corridors in Figure 4 to Figure 8, we can see that the calculated values mostly fell inside of the measurement uncertainty of the measured values. When considering this, it must be taken into account that during the measurements the pallet racks were almost fully occupied. The material stored on the pallets was a mix of small to medium plastic and metallic items stored mostly in cardboard boxes, which were placed on wooden pallets stored on the racks. The exact content of the items stored at each part of the racks was not known. Furthermore, some racks were fully loaded, whereas on some racks some pallets were missing and/or some pallets were not fully loaded. Thus, it can be expected that the racks' attenuation and reflection of the EMF was highly inhomogeneous. To further complicate the matter, very limited data are available regarding the attenuation and reflection of such occupied pallet racks at the frequency of 3500 MHz. Therefore, the attenuation for the NARDA tool was determined through a parametric study, and reflection coefficients for the MATLAB 1 tool were assigned uniformly for all packages corresponding to cardboard. If we analyze the results along corridor 3 in Figure 6, we can see that the NARDA model underestimated the values at distances of about 70 to 80 m. This means that there, the real value of the attenuation of pallet racks was lower than 3 dB, as higher measured values were due to the contribution of pRRHs in corridor 2. However, if we focus on corridor 2 in Figure 5, we can see that the NARDA model overestimated the values at distances of about 40 to 50 m. This means that there, the real value of the attenuation of pallet racks was higher than 3 dB, as higher calculated values were due to the contribution of pRRHs in the corridor 2, which in reality was lower than modeled. These cases clearly show that attenuation of the pallet racks significantly affects the results locally.

In Table 2 the validation results for the point-to-point comparison are presented. The Narda tool satisfied the validation criterion, with the difference between measured and calculated values remaining within the expanded measurement uncertainty for 87.5% of the evaluation points. On the contrary, the matlab tool did not meet criterion, as in only 57.5% of the evaluation points that the estimated e-field was within the measurement uncertainty. As mentioned earlier, this is attributed to the fact that it didn't account for ray transmission through the objects placed on the racks which in combination with the fact that the 3d model of the warehouse did not accurately represent the volume of the rack contents, resulted in unrealistically high attenuation values.

Table 2. Point-to-point comparison validation results

	measurements	NARDA 40 points	Matlab 2 40 points
number of samples	40	40	40
Uncertainty [dB]	3.5	-	-
Number of valid points $\lvert Diff_{point} \rvert < U_{meas,point}]$		**35**	**23**
Percentage of valid points		87.5	57.5
Validation result		Pass	Fail

In Table 3 the validation results for the general exposure-characterization comparison are presented. For the Narda tool, the En score for both percentiles ranged between -1 and 1, meaning that the validation criterion was met. For the matlab tool, only the 95th percentiles were within the required range showing satisfactory performance in estimating the higher values of the distribution. In contrast, the validation criteria were not met for the 50th percentile, as the tool significantly underestimated the electric field in areas that were blocked by the racks which had an effect on the median value.

Table 3. General exposure-characterization comparison validation results

	measurements	NARDA	Matlab 2
number of samples	40	40	40
Bootstrap samples	1000	1000	1000
E50 [V/m]	0.39	0.37	0.2
U50 [V/m]	0.1	0.06	0.11
En,50 score	-	**-0.17**	**-1.26**
E95 [V/m]	1.01	0.98	0.85
U95 [V/m]	0.42	0.28	0.28
En,95 score	-	**-0.06**	**-0.33**
Validation result	-	**Pass**	**Fail**

3.2 Scenario 2: Smart Industry 4.0: Production Hall, private SA 5G FR1

At a production site for electronic device assembly and testing, a private 5G network was installed. 4 small cell access points are mounted on the ceiling and 2 are mounted on the indoor

balcony. All of them are operating in the range 3700–3800 MHz with a maximum output power of 1 W. Details about the setup are given in deliverable D 2.2.

Results obtained by measurements and by numerical calculations are given in Table 4.

Table 4. Results of measurements and numerical calculations with comparison to measurement values. For calculations, values are given for two datasets: same 36 points as measurements (36 points) or all calculated points at the height of 1.5 m (all).

	measurements	NARDA 36 points	NARDA all
number of samples	36	36	275678
maximum value [V/m]	2.11	1.78	2.72
95th percentile [V/m]	**1.22**	**1.37**	**1.14**
75th percentile [V/m]	0.96	0.94	0.91
mean value [V/m]	0.84	0.91	0.79
median value [V/m]	**0.66**	**0.81**	**0.74**
25th percentile [V/m]	0.52	0.71	0.50
standard deviation [V/m]	0.88	0.80	0.77
quartile coefficient of dispersion	0.30	0.14	0.29
root mean square error [v/m]		0.30	
normalized root mean square error		0.36	
Pearson correlation coefficient r		0.60	
Pearson correlation coefficient p		0.00	
Kolmogorov-Smirnov (K-S) test D-stat		0.25	0.15
Kolmogorov-Smirnov (K-S) test D-crit 0.05		0.32	0.23

From the results it is evident that the correlation between the measurements and results of model is present but not very strong, as the r-value is 0.60 and p value is below 0.05. Results for 95th percentile, 75th percentile, mean value and 25th percentile agree well with differences typically below 20%.

Kolmogorov-Smirnov test and cumulative distribution plot in in Figure 9 showed good agreement between the cumulative distributions of all result. They showed also that the selected 36 points represent the distribution of the electric field inside the analyzed area well, as cumulative distribution plots for all calculation points agree well with those for 36 points.

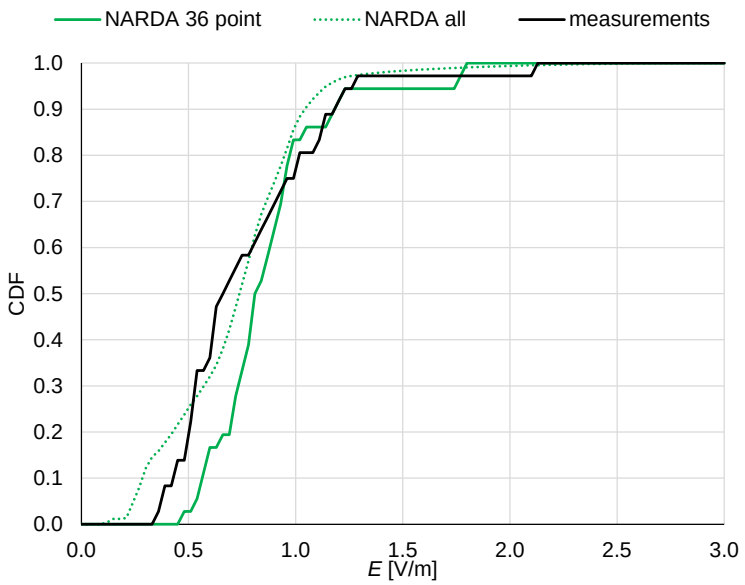

Figure 9. Cumulative distribution of measurements and calculations.

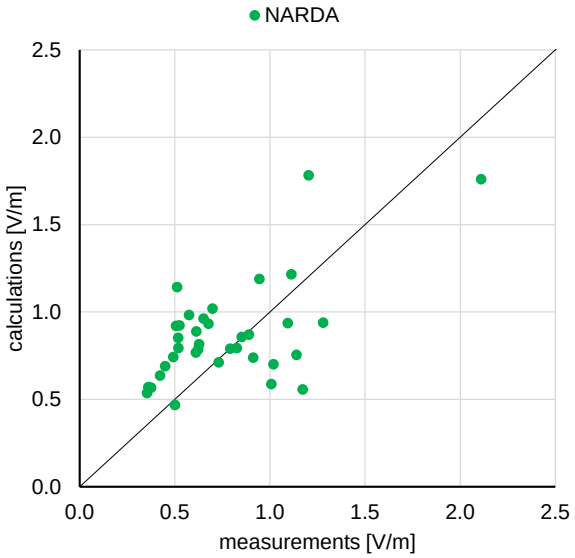

Figure 10. Scatter plots of measured values (x axis) and calculated values (y axis).

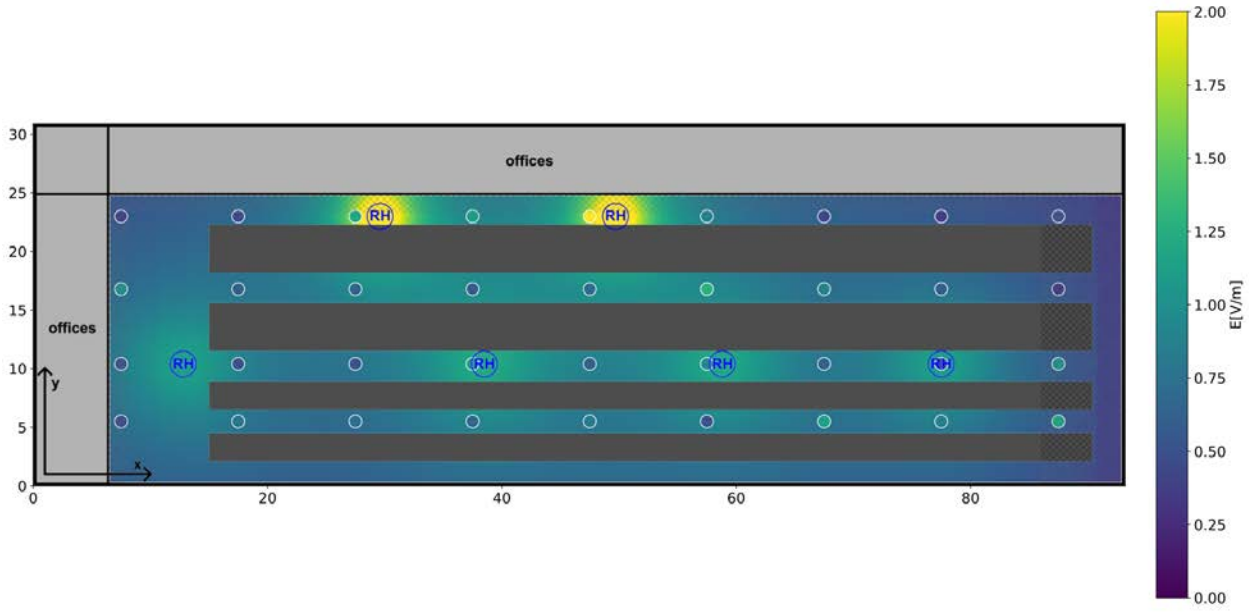

Figure 11. Results of calculations (colored layer) and measurements (dots with white border).

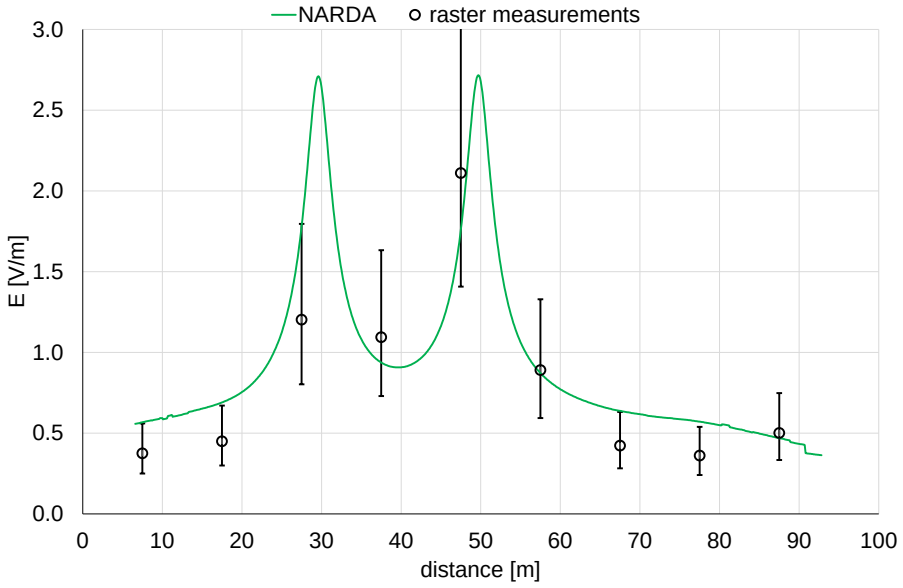

Figure 12. Electric field values along corridor 1. The results are given for the extrapolated maximum value. Circles represent the values measured during raster measurements together with measurement uncertainty. The distance is the distance along the corridor starting at the very left end of the Figure 11.

From the comparisons of results of measurements and calculations along the corridors in Figure 12 to Figure 15, we can see that the calculated values mostly fell inside of the measurement uncertainty of the measured values or are just slightly out of this range.

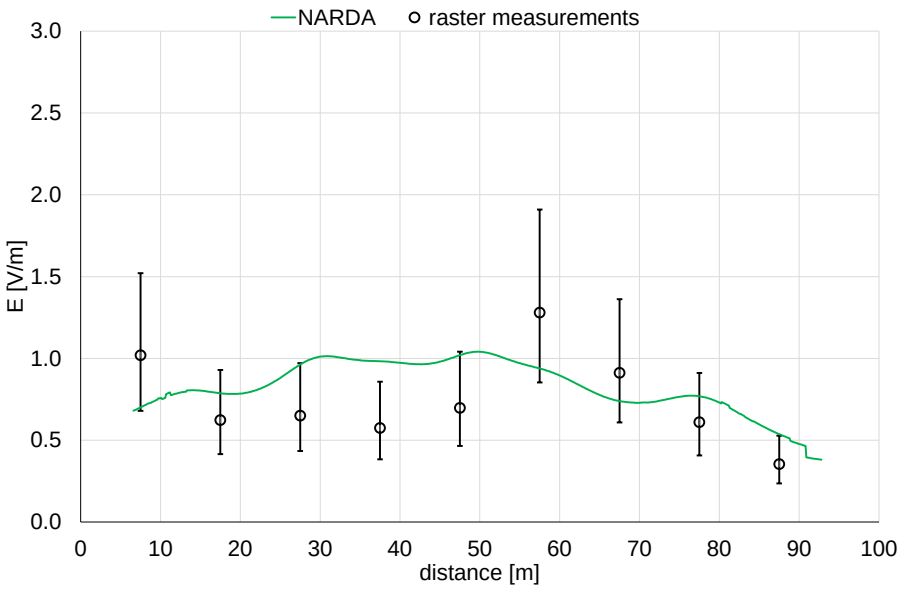

Figure 13. Electric field values along corridor 2. The results are given for the extrapolated maximum value. Circles represent the values measured during raster measurements together with measurement uncertainty. The distance is the distance along the corridor starting at the very left end of the Figure 11Figure 3.

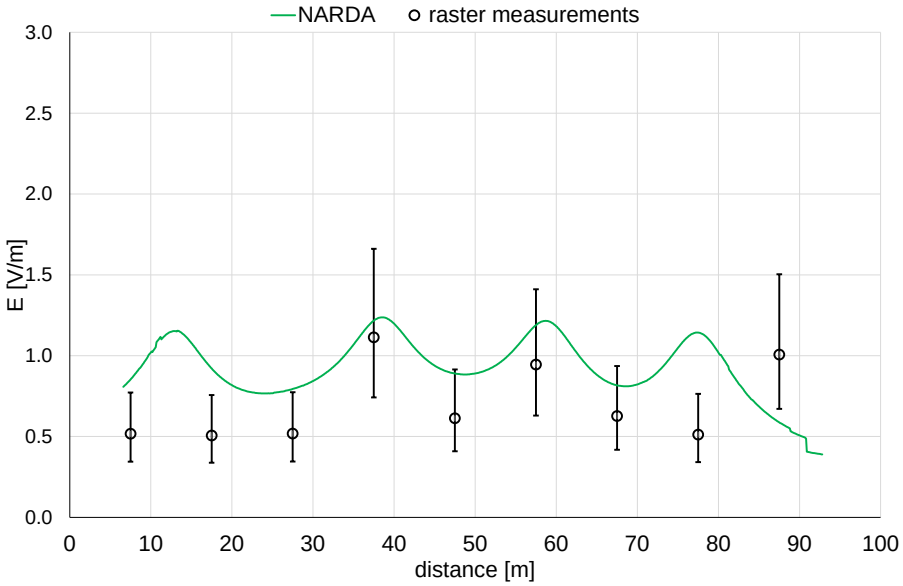

Figure 14. Electric field values along corridor 3. The results are given for the extrapolated maximum value. Circles represent the values measured during raster measurements together with measurement uncertainty. The distance is the distance along the corridor starting at the very left end of the Figure 11.

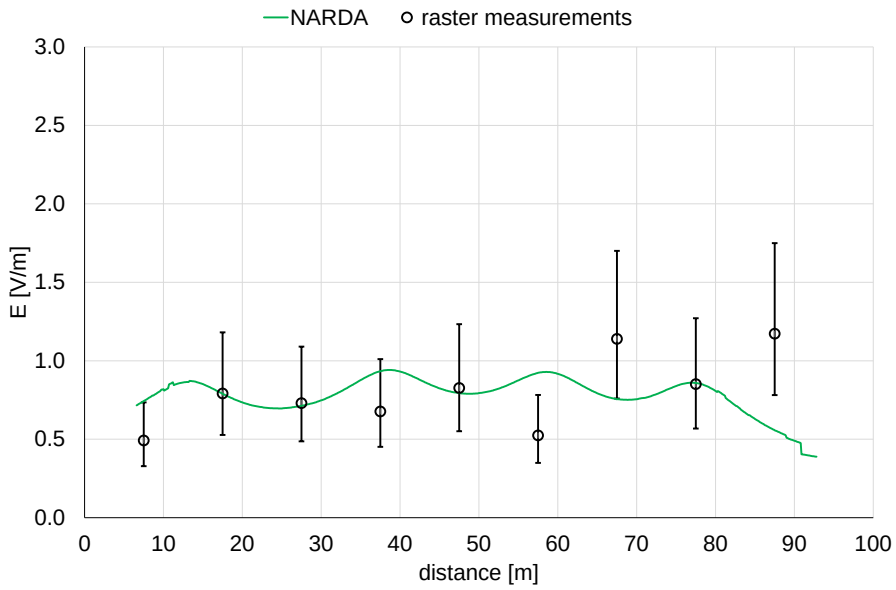

Figure 15. Electric field values along corridor 4. The results are given for the extrapolated maximum value. Circles represent the values measured during raster measurements together with measurement uncertainty. The distance is the distance along the corridor starting at the very left end of the Figure 11.

In Table 5 the validation results for the point-to-point comparison are presented. The Narda tool used for the calculations barely missed the validation mark as the percentage of evaluation points where the difference between measured and calculated values was below the measurement uncertainty was 63.9% instead of 68%.

Table 5. Point-to-point comparison validation results

	measurements	NARDA
number of samples	36	36
Uncertainty [dB]	3.5	-
Number of valid points ($\|Diff_{point}\| < U_{meas,point}$)		**23**
Percentage of valid points		63.9
Validation result		Fail

In Table 6 the validation results for the general exposure-characterization comparison are presented. The En scores for the 50th and 95th percentiles were within the required range of –1 to 1.

Table 6. General exposure-characterization comparison validation results

	measurements	NARDA 36 points
number of samples	36	36
Bootstrap samples	1000	1000
E50 [V/m]	0.66	0.81
U50 [V/m]	0.14	0.08
En,50 score	-	**0.88**
E95 [V/m]	1.22	1.37
U95 [V/m]	0.52	0.53
En,95 score	-	**0.18**
Validation result	-	**Pass**

3.3 Scenario 3: Research laboratory, private NSA 5G FR2

In a research facility a private test 5G network is installed in an anechoic chamber. Private NSA 5G FR 2 network operates in the frequency range of 25.5-25.9 GHz. The Nokia AWEUC AirScale radio head is mounted on the movable pole at the height of 1.5 m. The power delivered to antenna was 1 W. Details about the setup are given in deliverable D 2.2.

Detailed information regarding the installation is given in Table 7.

From the results it is evident there is a good correlation between the measurements and results of models, as the r-value is 0.99 for both models and p value is below 0.05. Results for 95th percentile, 75th percentile, mean value and 25th percentile agree well when comparing both models, but the results of measurements are slightly higher compared to results of numerical modelling.

Kolmogorov-Smirnov test and cumulative distribution plot in Figure 16 showed good agreement between the cumulative distributions of result at 9 points. There is significant difference to the results of numerical calculations for the whole model and they do not agree well with the results of measurements. The reason for this is the fact that for this scenario no raster measurements were done. Therefore, for the purpose of the validation, results of measurements in the main beam of the antenna were used. When comparing the results on the same 9 locations as measurements were done, they agree well. But when comparing a whole set of results of numerical calculations, the differences are significant. Based on this we can conclude that the electric field values in main beam does not represent the exposure inside the whole analyzed area. As expected, in main beam direction the values are higher compared to other directions, which reflects also in significantly lower 95th percentile, 75th percentile, mean value and 25th percentile for results with all points in Table 7.

Table 7. Results of measurements and numerical calculations with comparison to measurement values. For calculations, values are given for two datasets: same 9 points as measurements (9 points) or all calculated points at the height of 1.5 m (all).

	measurements	MATLAB 2 9 points	NARDA 9 points	MATLAB 2 all	NARDA All
number of samples	9	9	9	14161	14641
maximum value [V/m]	59.65	39.33	41.66	65535.00	244.19
95th percentile [V/m]	**48.44**	**32.92**	**34.55**	**14.24**	**13.23**
75th percentile [V/m]	16.24	13.23	12.52	6.35	5.32
mean value [V/m]	23.48	16.47	16.73	550.80	8.99
median value [V/m]	**11.69**	**8.38**	**7.38**	**3.38**	**2.61**
25th percentile [V/m]	8.75	6.27	5.23	0.92	0.30
standard deviation [V/m]	33.73	22.17	23.62	6007.58	29.94
quartile coefficient of dispersion	0.30	0.36	0.41	0.75	0.89
root mean square error [v/m]		7.27	0.57		
normalized root mean square error		0.31	0.02		
Pearson correlation coefficient r		0.99	0.99		
Pearson correlation coefficient p		0.00	0.00		
Kolmogorov-Smirnov (K-S) test D-stat		0.33	0.44	0.74	0.81
Kolmogorov-Smirnov (K-S) test D-crit 0.05		0.64	0.64	0.45	0.45

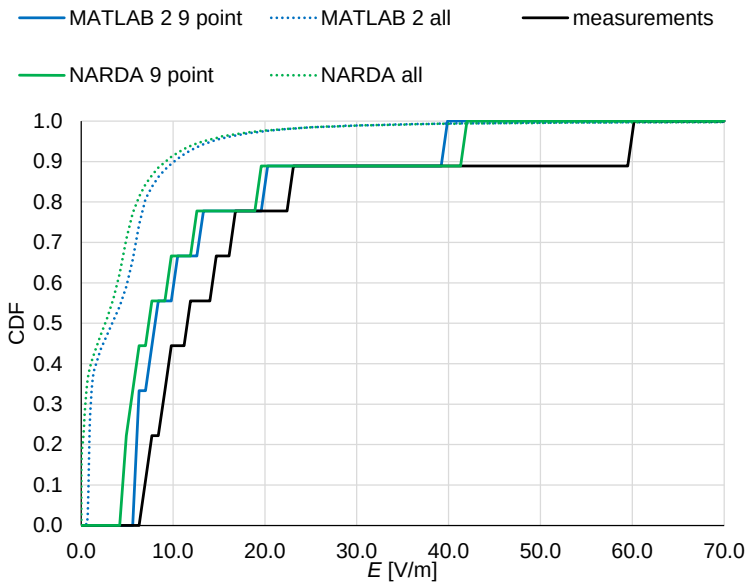

Figure 16. Cumulative distribution of measurements and calculations.

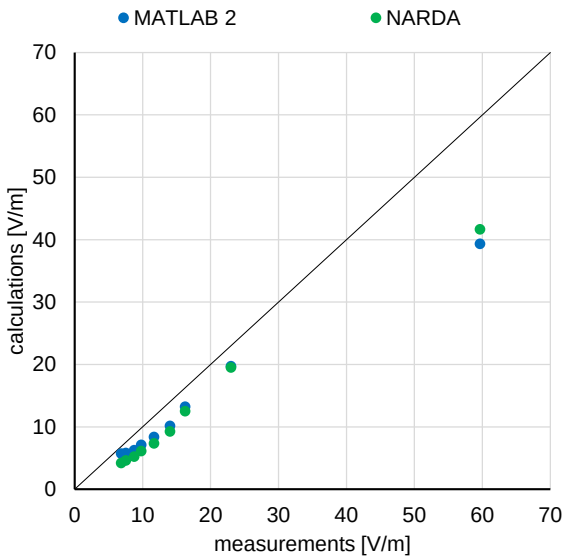

Figure 17. Scatter plots of measured values (x axis) and calculated values (y axis).

In Table 8 the validation results for the point-to-point comparison are presented. The calculated E-field values with both numerical tools fell within the expanded measurement uncertainty for each one of the 9 evaluation points.

Table 8. Point-to-point comparison validation results

	measurements	NARDA	Matlab 2
number of samples	9	9	9
Uncertainty [dB]	3.5	-	-
Number of valid points $[\lvert Diff_{point}\rvert < U_{meas,point}]$		**9**	**9**
Percentage of valid points		100%	100%
Validation result		Pass	Pass

Table 9. General exposure-characterization comparison validation results

	measurements	NARDA	Matlab 2
number of samples	9	9	9
Bootstrap samples	1000	1000	1000
E50 [V/m]	11.69	7.38	8.38
U50 [V/m]	6.79	6.19	5.98
En,50 score	-	**-0.41**	**-0.37**
E95 [V/m]	48.44	41.66	32.92
U95 [V/m]	31.36	23.34	18.69
En,95 score	-	**-0.41**	**-0.37**
Validation result		**Pass**	**Pass**

In Table 9 the validation results for the general exposure-characterization comparison are presented. For both numerical tools, the En scores for both percentiles ranged between –1 and 1, indicating that the validation criterion was met. As in the first scenario, the combination of a small dataset and the presence of one measurement value much larger than the rest led to high uncertainty values, particularly for the 95th percentile. This, in turn, made it easier for the criterion to be satisfied. In any case, the performance of both numerical models is considered successful, primarily because they also met the more stringent validation criterion of the point-to-point comparison.

3.4 Scenario 4: Wi-Fi 6

For the 7th scenario, measurements and simulations were conducted in a university laboratory where a Wi-Fi 6 access point is installed operating in the 5 GHz frequency band with a maximum transmit power of 23 dBm. The access point (AP) is positioned on top of a table at a height of approximately 1 m above the floor. Details about the setup are given in deliverable D 2.3. Raster measurements were carried out under maximum-traffic conditions. A total of 88 measurement points were distributed within the laboratory's free space, with a spacing of 0.5 m between adjacent points. All measurements were taken at a sensor height of 1.1 m. The electric field at the measurement positions was estimated using the numerical tool Matlab 1 (phasor sum).

The measurement and simulation results are presented in Table 10.

Table 10. Results of measurements and numerical calculations with comparison to measurement values

	measurements	MATLAB 1
number of samples	88	88
maximum value [V/m]	5.2	5.67
95th percentile [V/m]	**2.67**	**3.34**
75th percentile [V/m]	1.55	2.12
mean value [V/m]	1.58	1.67
median value [V/m]	**1.3**	**1.38**
25th percentile [V/m]	0.91	0.93
standard deviation [V/m]	0.74	1.01
quartile coefficient of dispersion	0.26	0.39
root mean square error [v/m]		0.96
normalized root mean square error		0.64
Pearson correlation coefficient r		0.56
Pearson correlation coefficient p		0.00
Kolmogorov-Smirnov (K-S) test D-stat		0.17
Kolmogorov-Smirnov (K-S) test D-crit 0.05		0.21

From the results in Table 10, it can be seen that the differences in key statistics, such as the 25th, 75th, and 95th percentiles, as well as the mean, median, and maximum, do not exceed 21%. The Pearson correlation coefficient indicates a moderate linear correlation between the measured and calculated electric field values, with an r-value of 0.56 and a p-value of 0. The Kolmogorov-

Smirnov and the cdf plots presented in Figure 18 demonstrate a relatively good fit between the two datasets.

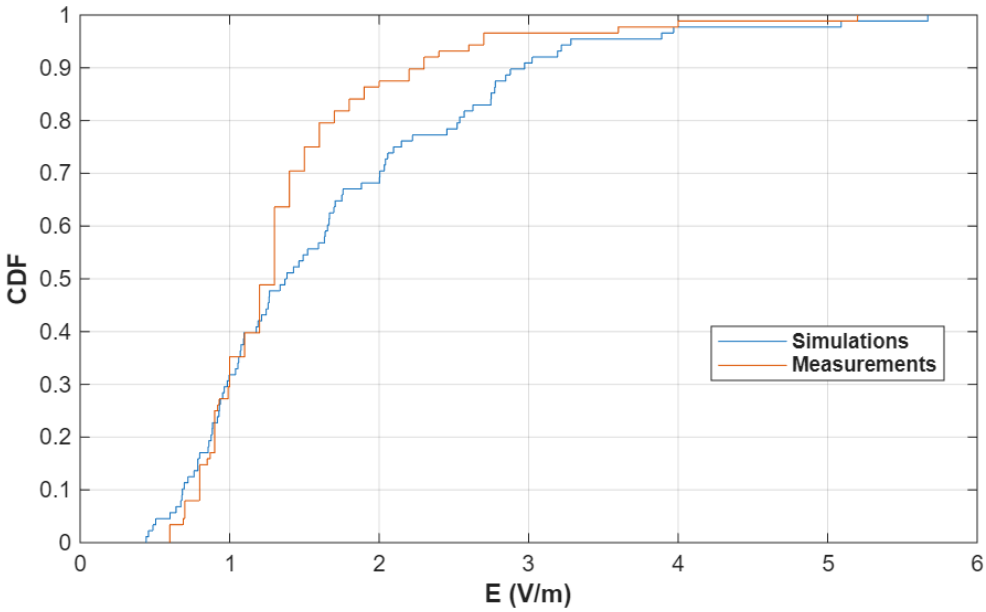

Figure 18. Cumulative distribution of measurements and calculations.

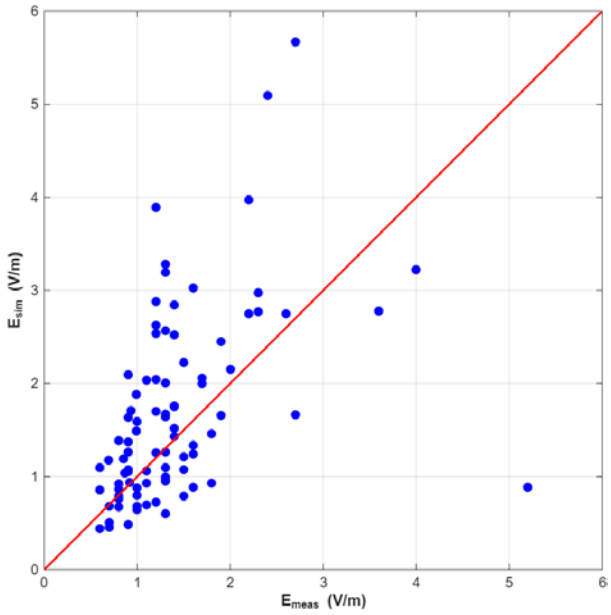

Figure 19. Scatter plots of measured values (x axis) and calculated values (y axis).

For the point-to-point comparison, the measurement standard uncertainty was 24.32%. For this scenario it was attempted to estimate the simulation uncertainty as well. There are several factors that contribute to the model's uncertainty and have an effect on the calculated e-field,

such as the transmitter's power and radiation pattern, the inaccuracy of the environment that is created and the uncertainty in determining the exact position of the measurement points. Particularly the positioning uncertainty plays a major role in the e-field calculations that can vary significantly between adjacent positions due to the constructive and destructive interference of the rays that arrive at the evaluation point. To estimate the effect of positioning uncertainty on the calculated electric field, the field was calculated at 100 random points within a sphere of radius equal to one wavelength (5.7 cm) around each nominal evaluation point. This radius corresponds approximately to the physical size of the measurement probe's radome and represents the expected positional uncertainty in the measurements. Assuming that the actual measurement location has an equal probability of lying anywhere within this sphere, the electric field is considered uniformly distributed over the range of the calculated values. The standard uncertainty is then:

$$u_{pos,point} = \frac{E_{sphere,max} - E_{sphere,min}}{2\sqrt{3}}$$

The simulation standard uncertainty varies across evaluation points, with relative values ranging from 12% to 57%, with a mean value of 41.38%. The mean value of the combined relative standard uncertainty is then 48%, which is very close to the expanded measurement uncertainty of 47.67%.

In Table 11 the validation results for the point-to-point comparison are presented. The matlab tool used for the calculations satisfied the validation criterion, as the difference between measured and calculated values was smaller than the combined standard uncertainty for 62 of the 88 evaluation points.

Table 11. Point-to-point comparison validation results

	measurements	**Matlab 1**
number of samples	88	88
Standard Uncertainty [%]	24.32	41.38 (mean)
Number of valid points ($\|Diff_{point}\| < u_{c,point}$)		**62**
Percentage of valid points		70.46
Validation result		Pass

In Table 12 the validation results for the general exposure-characterization comparison are presented. The En score for both percentiles examined ranged between -1 and 1, meaning that the validation criterion was met.

Table 12. General exposure-characterization comparison validation results

	measurements	Matlab 1
number of samples	88	88
Bootstrap samples	1000	1000
E50 [V/m]	1.3	1.38
U50 [V/m]	0.1	0.28
En,50 score	-	**0.26**
E95 [V/m]	2.7	3.34
U95 [V/m]	1.04	1.07
En,95 score	-	**0.43**
Validation result		**Pass**

3.5 Validation conclusions

Different numerical models were used for exposure estimation in 4 scenarios and their results were compared with extensive measurement data. The differences were evaluated through point-to-point comparisons and for a general exposure-characterization.

For the point-to-point comparison, the results showed that, for the majority of measurement points, the calculated values were within the measurement uncertainty. The validation criterion of 68% for each scenario was met by the Narda tool in the 'Warehouse' case (scenario 1), by both the Narda and Matlab tools in scenario 3 and by the Matlab tool in scenario 4. In the remaining cases the models failed to meet the validation criterion due to inaccuracies in modeling the transmitting antennas and the environment as well as due to the inability in determining the exact measurement positions.

For the general exposure-characterization, the results showed that the numerical models accurately estimated the typical and high-end exposure levels within the examined environments. The validation criterion was satisfied for all numerical tools in all scenarios with the exception of the Matlab tool in the warehouse case (scenario 1), where inaccuracies in modelling the racks led to an underestimation of the typical exposure (median value).

Overall, it can be concluded that the numerical tools perform well in estimating general exposure levels and with sufficiently detailed modeling of the environment and EMF sources can accurately estimate the electric field at specific locations.

Results of validation clearly shows that results of numerical models are valid for the indoor exposure estimation. Mostly point to point results were within the uncertainty of the measurement equipment, whereas the final statistical results, like 95th percentile and median value, were within the 20% difference. When considering this, it must be taken into account the complexity of some of the analyzed scenarios with many obstacles, walls, ceiling and floor, which all influence the calculated value.

4 Validation of generic model

The generic model was tested using experimental data collected in three scenarios, which were described in detail in D2.2. The corresponding experimental datasets are extensively documented in D2.3. Since the outputs of the generic model are the median and 95th percentile electric field values representing the entire occupational environment, raster measurements were used for the validation to ensure uniform coverage of the area of interest. However, because measurements cannot provide detailed coverage over large areas such as those considered in these scenarios, the generic model results were also compared with corresponding values obtained from calculations using the Narda numerical tool. In these calculations, the E-field was evaluated on a much finer grid, comprising orders of magnitude more points than the measurements. The Narda tool was used for the validation of the generic model for two reasons: first, because, as shown in the previous section, it has been validated for these scenarios, and second, because unlike the Matlab tool, its results were not used to train the generic model, ensuring an independent validation. It should be noted that in the previous section the numerical tool results were based only on the measurement locations, while here the median and 95th percentile values were derived from calculations over a much denser set of points, providing a more detailed representation of the entire area.

Table 13. Descriptive parameters of the three experimental datasets. Parameters in italic & bold (X3, X5, X6, X7, X8) are actually used as inputs to the generic model.

	Value		
	Smart Industry 4.0: Warehouse	**Smart Industry 4.0: Production hall**	**Office, test facility of wireless networks**
X1 - environment size (m²)	3398.6	2116.8	399
X2 - number of transmitters (-)	4	6	1
X3 - transmitter density (/100m²)	0.118	0.283	0.251
X4 - frequency (GHz)	3.75	3.75	3.47
X5 - antenna height (m)	5	5.9*	3
X6 - transmit power (dBW)	1	1	20
X7 - antenna type/location	Ceiling (omni)	Ceiling (omni)	Wall (half-omni)
X8 - clutter area percentage (%)	40	20	0
X9 - dominant clutter material	Metal	Metal	-
X10 - outer wall material	Concrete	Concrete	Concrete
X11 - ceiling height	5.5	6.9	5.6

*Two antennas were mounted at the height of 3.1 m.

Table 13 presents the parameters characterizing the environments that were initially considered as inputs to the generic model. As described in D2.2, only parameters X3, X5, X6, X7, and X8 were ultimately retained for the model implementation. In the “Production Hall” scenario, base station antennas were installed at two heights, but since the generic model requires a single input value for antenna height, height of 5.9 m was used, as 4 out of 6 antennas are mounted at that height.

Table 14 presents the outputs of the generic model for each environment in which it was tested, along with the corresponding parameter values obtained from the measurement datasets and from the simulation datasets produced using the Narda numerical tool.

Table 14. Comparative output of simulation and measurements with generic model estimations.

Output parameter	Method	Smart Industry 4.0: Warehouse	Smart Industry 4.0: Production hall	Office, test facility of wireless networks
E50 (V/m)	Simulations NARDA	0.34	0.74	4.01
	Measurements	0.39	0.66	5.05
	Generic model	0.24	0.75	4.10
E95 (V/m)	Simulations NARDA	1.06	1.14	11.31
	Measurements	1.01	1.22	10.74
	Generic model	1.21	1.34	8.23
kurtosis	Simulations NARDA	1.94	3.84	1.61
	Measurements	1.97	4.68	-0.64
	Generic model	1.57	0.09	2.90

In Figure 20 the median and 95th percentile values obtained from the generic model, the measurements and simulations are plotted. The error bars represent the expanded uncertainty of the E50 and E95 statistics obtained from the measurement dataset using the bootstrapping method. The uncertainty values for each statistic at each scenario are presented in the corresponding paragraph of chapter 3 Validation of various exposure scenarios.

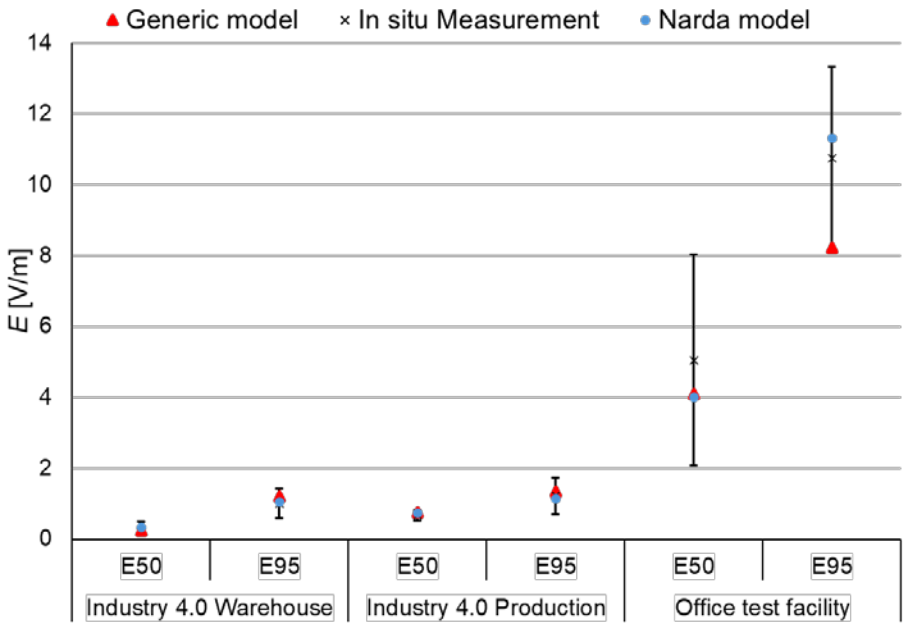

Figure 20. Comparison of results obtained by generic model (red triangles), simulations (blue circles) and measurements (black x)

Overall, there is good agreement between the generic model results and the measurements for the 50th (median) and 95th percentiles. Only one value fell outside the uncertainty range: the

median E-field in the warehouse case, where the generic model's output was 0.24 V/m, which is lower than the uncertainty range's lower limit of 0.29 V/m (the actual value was 0.39 V/m). Another case where the generic model did not perform too well was for the 95th percentile in the office scenario. Here, the model's value of 8.23 V/m was near the edge of the uncertainty range compared to the value of 10.74 V/m obtained from the measurements, but it remained inside the margin. For all other cases, the generic model agreed very well with the measurements, with relative differences not exceeding 20%.

The same conclusions are drawn when comparing the generic model results with simulations. For the median value of the 'Warehouse' case, the relative difference between the two models was 29% (0.24 and 0.34 V/m respectively). Although this percentage appears relatively high, it is mainly due to the low absolute field strengths. The absolute difference of 0.1 V/m is generally not considered significant in the context of RF human exposure assessment. For the 95th percentile value of the 'Office' case the relative difference was similar, at 27% (8.23 and 11.31 V/m). This relatively high difference is attributed to the large antenna directivity (11.19 dBi) in the 'Office' scenario, which was outside the range of the data used for the training of the generic model. In all other cases the agreement was very good, with relative differences below 17%. The results also show that the values obtained from the simulations and the measurements agreed very well, indicating that, despite the limited number of measurement points, the measurements provided a representative characterization of the overall exposure in each environment.

For the kurtosis the generic model results did not agree well with neither measurements nor simulations. This was expected since, as shown in D2.2, the reliability of this statistic was found to be weak on the model performance tests.

From the results, it can be concluded that the generic model is capable of accurately approximating not only simulated scenarios but also measured E-field values in real environments. However, it was observed that the model's accuracy decreases when the input parameters fall outside the range covered during the training phase. This suggests that the model's performance can be further improved by incorporating additional and more complex training environments, thereby expanding the input parameter space through a broader set of configurations. To support the continued development and refinement of a generic exposure model, the simulated and experimental datasets will be made publicly available, enabling researchers to add new experimental data, refine the existing model, or even propose alternative modeling approaches.

5 Compliance boundaries of emissions from New Local Networks in Industry 4.0.

For each antenna considered in the simulations, the compliance boundaries were determined by evaluating the compliance distance in all directions around the antenna. Compliance Distance (CD) is the minimum distance from the antenna at which the power density no longer exceeds the reference level limit S_{lim}. We derive *CD* using the spherical far-field formula for power density:

$$S(r,\theta,\varphi) = \frac{P \cdot G(\theta,\Phi)}{4\pi r^2},$$

Where *S* is the radiated power density (W/m²), *P* is the input power to the antenna (W), $G(\vartheta,\Phi)$ is the linear gain of the antenna (-), *r* is the radial distance from the antenna (m), ϑ is the polar (elevation) angle, and Φ is the azimuthal angle.

Solving the above equation for *r*, we can determine *CD*:

$$CD(\theta,\varphi) = \sqrt{\frac{P \cdot G(\theta,\varphi)}{4\pi S_{lim}}}$$

This equation provides the direction-dependent compliance distance $CD(\vartheta,\Phi)$, which varies according to the antenna's radiation pattern. Using this formulation, we compute the 3D iso-surface compliance boundary, which defines the smallest closed surface surrounding the antenna where the power density equals S_{lim} in all directions. Additionally, we derive the box-shaped compliance boundary, defined as the smallest axis-aligned bounding box that entirely encloses the 3D iso-surface. This box provides a simplified geometric representation useful for compliance zoning.

The figures in the following paragraphs show the 3D iso-surface plot of the compliance boundary, along with the vertical and horizontal cross-sectional cuts of the compliance distance for each antenna used in our simulations. For the horizontal cut, the polar angle (ϑ) was selected such that the absolute value of the compliance distance in the x-direction, $|CD_x|$, was maximized. For the vertical cut, the azimuth angle (Φ) was chosen to maximize the absolute value of the compliance distance in the z-direction, $|CD_z|$. It is noted that the figures were produced taking into account the general public exposure limits.

Table 15 summarizes the vertical and horizontal compliance distances for all examined scenarios. For general public and occupational exposure, the applied power density limits are 10 W/m^2 and 50 W/m^2, respectively, as established by ICNIRP [14] and in accordance with the EU directive 2013/35/EU [11].

Table 15. Compliance Distances across simulation scenarios for general public and occupational exposure

Simulation Scenario	Antenna model	Input power (W)	General public exposure S_{lim} = 10 W/m²		Occupational exposure S_{lim} = 50 W/m²	
			Vertical Compliance Distance [m]	Horizontal Compliance Distance [m]	Vertical Compliance Distance [m]	Horizontal Compliance Distance [m]
FR1: 3.5 GHz – common scenario	Alpha Wireless AW3232	4	0.17	0.89	0.07	0.4
FR1: 3.6 GHz – indoor smart Industry 4.0	Nokia AirScale Pico	1	0.09	0.09	0.04	0.04
FR1: 3.5 GHz – Port of Koper, outdoor macro cell	Ericsson AIR3227	100	2.43	13.27	1.09	5.94
FR1: 3.5 GHz – Office, small cell	Ericsson 6524	16	0.39	1.27	0.17	0.57
3.5 GHz – Indoor warehouse Ghent	FR1 omni-BS	12.59	0.18	0.4	0.08	0.18
WiFi 6: 5.5 GHz – lab scenario, beamforming	Cisco Catalyst 9115E	0.2	0.15	0.05	0.07	0.02
FR2: 26 GHz – Lab scenario, beamforming	Nokia AWEUC	1	0.38	1.4	0.17	0.62
FR2: 28 GHz – Indoor warehouse, beamforming	5G NR 2x2	1	0.1	0.29	0.05	0.13
	5G NR 4x4		0.12	0.6	0.05	0.27
	5G NR 6x6		0.13	0.91	0.06	0.41
	5G NR 8x8		0.14	1.23	0.06	0.55
	5G NR 10x10		0.14	1.54	0.06	0.69

From the results of the compliance distance calculations, it is evident that there is a substantial difference between the indoor antennas used in the various scenarios and the outdoor antenna employed in the macrocell scenario at the Port of Koper.

For indoor antennas, the vertical compliance distances range from 9 to 39 cm for general public exposure and from 4 to 17 cm for occupational exposure. The horizontal compliance distances range from 9 cm to 1.54 m for general public exposure and from 4 to 69 cm for occupational exposure.

For the outdoor antenna, the vertical compliance distances are increased by at least a factor of six, reaching 2.43 m and 1.09 m for general public and occupational exposure, respectively. Similarly, the horizontal compliance distances are increased by at least a factor of nine, reaching 13.27 m and 5.94 m for general public and occupational exposure, respectively.

5.1 Logistic sector: Port of Koper, private 5G FR1

The current exposure scenario is based on a private 5G FR1 base station located in Port of Koper, Slovenia. Full technical description can be found in D 2.2. The compliance boundaries of the modelled antenna are presented in Figure 21.

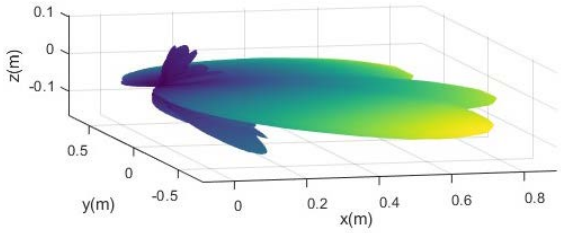

(a) Iso-surface

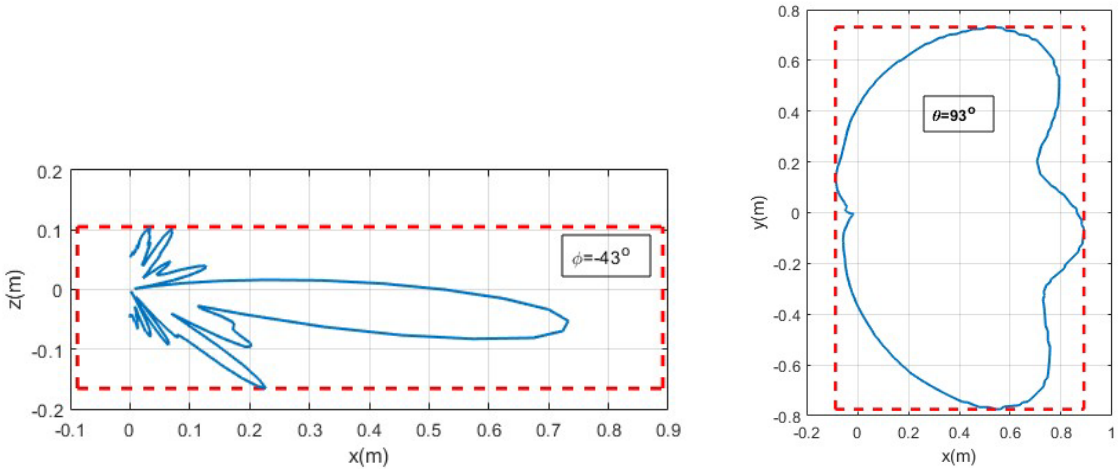

Vertical cut (φ=-43°) and horizontal cut (ϑ=93°): compliance distance (blue line) and box-shaped compliance boundary (red dashed line)

Figure 21. Compliance boundaries for Alpha Wireless AW3232 Base Station sector antenna assuming 4 W transmitted power.

5.2 Smart Industry 4.0: Warehouse and Production Hall

The current exposure scenario is based on a private 5G FR1 pico base station located in a Smart industry warehouse and production hall in Germany. Full technical description can be found in D2.2. The compliance boundaries of the modelled antenna are presented in Figure 22.

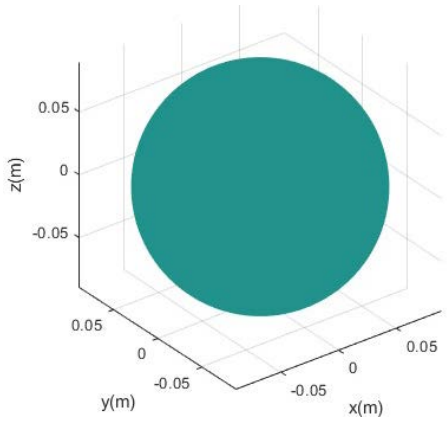

(a) Iso-surface

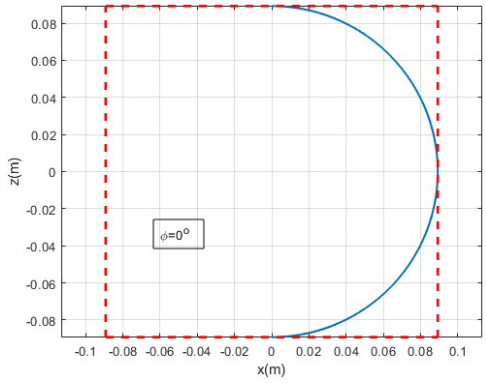

(b) Vertical cut (φ=0°): compliance distance (blue line) and box-shaped compliance boundary (red dashed line)

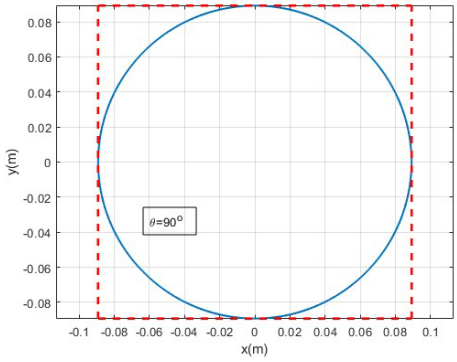

(c) Horizontal cut (ϑ=90°): compliance distance (blue line) and box-shaped compliance boundary (red dashed line)

Figure 22. Compliance boundaries for Nokia AirScale pico indoor remote radiohead assuming 1 W transmitted power.

5.3 Logistics sector: Port of Koper, public slice 5G FR1

The current exposure scenario is based on a slice of a public 5G FR1 base station located in Port of Koper, Slovenia. Full technical description can be found in D 2.2. The compliance boundaries of the modelled antenna are presented in Figure 23.

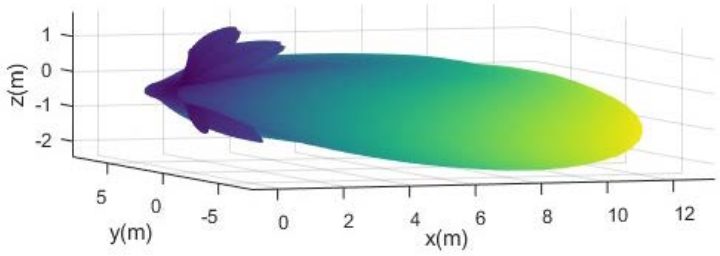

(a) Iso-surface

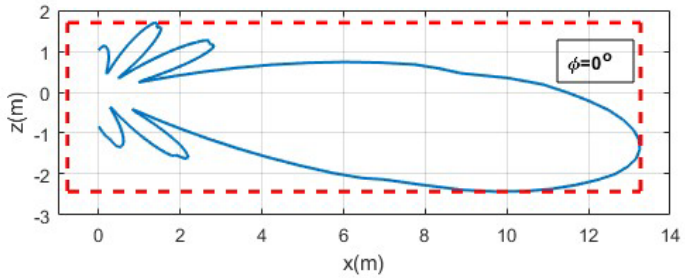

(b) Vertical cut (φ=0°): compliance distance (blue line) and box-shaped compliance boundary (red dashed line)

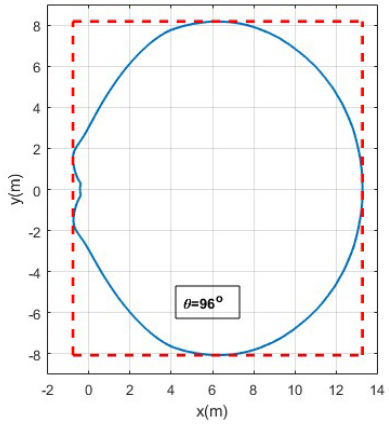

(c) Horizontal cut (ϑ=96°): compliance distance (blue line) and box-shaped compliance boundary (red dashed line)

Figure 23. Compliance boundaries for Ericsson AIR3227 antenna assuming 100 W transmitted power.

5.4 Office, test facility of wireless networks, private SA 5G FR1

The current exposure scenario is based on a private 5G FR1 base station located in an Office Hall. Full technical description can be found in D 2.2. The compliance boundaries of the modelled antenna are presented in Figure 24.

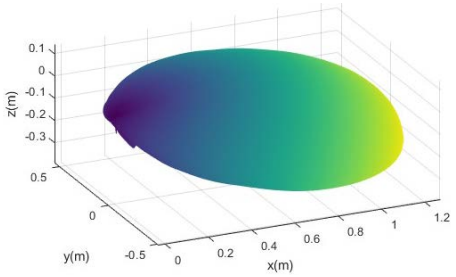

(a) Iso-surface

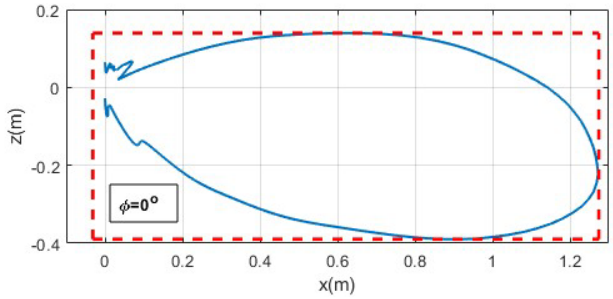

(b) Vertical cut (φ=0°): compliance distance (blue line) and box-shaped compliance boundary (red dashed line)

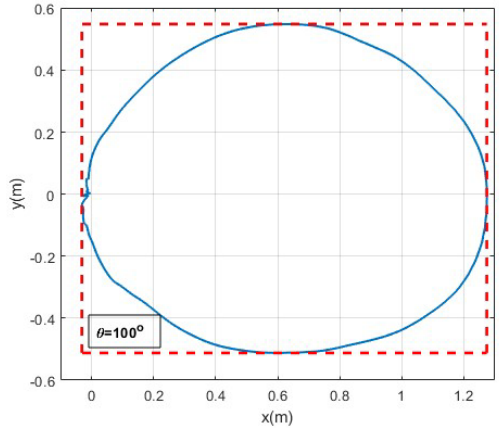

(c) Horizontal cut (ϑ=100°): compliance distance (blue line) and box-shaped compliance boundary (red dashed line)

Figure 24. Compliance boundaries for Ericsson 6524 antenna assuming 16 W transmitted power.

5.5 Logistics sector: Warehouse, private SA 5G FR1

The current exposure scenario is based on a private 5G FR1 base station located in a warehouse in Belgium. Full technical description can be found in D 2.2. The compliance boundaries of the modelled antenna are presented in Figure 25.

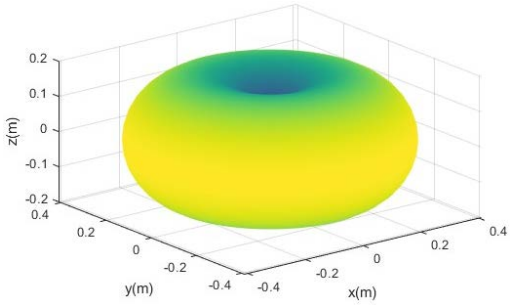

(a) Iso-surface

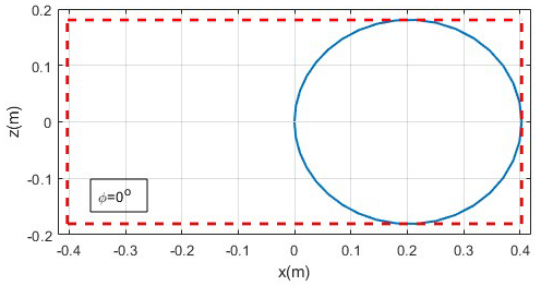

(b) Vertical cut (φ=0°): compliance distance (blue line) and box-shaped compliance boundary (red dashed line)

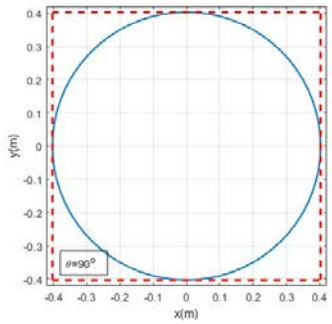

(c) Horizontal cut (ϑ=90°): compliance distance (blue line) and box-shaped compliance boundary (red dashed line)

Figure 25. Compliance boundaries for FR1 BS antenna assuming 12.59 W (41 dBm) transmitted power.

5.6 WiFi 6: 5.5 GHz – lab scenario, beamforming

The current exposure scenario is based on a Wi-Fi 6 access point located in Greece. Full technical description can be found in D 2.2. The compliance boundaries of the modelled antenna are presented in Figure 26.

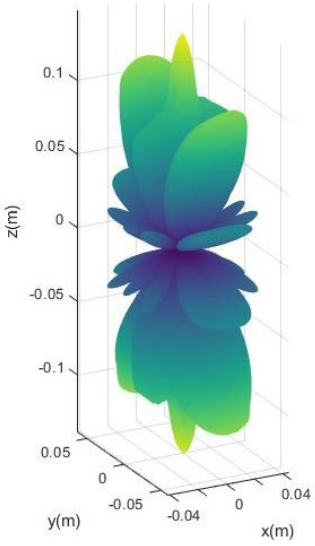

(a) Iso-surface

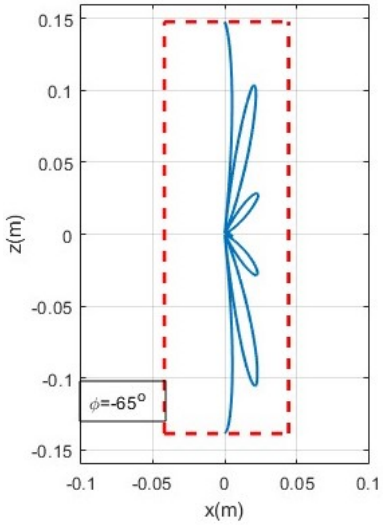

(b) Vertical cut (φ=-65°): compliance distance (blue line) and box-shaped compliance boundary (red dashed line)

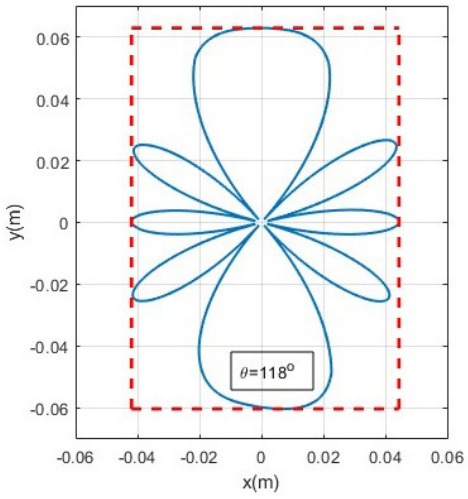

(c) Horizontal cut (ϑ=118°): compliance distance (blue line) and box-shaped compliance boundary (red dashed line)

Figure 26. Compliance boundaries for Cisco Catalyst 9115 antenna assuming 0.2 W transmitted power.

5.7 Research laboratory, private NSA 5G FR2, beamforming

The current exposure scenario is based on a private 5G FR2 base station located a research laboratory. Full technical description can be found in D2.2. The compliance boundaries of the modelled antenna are presented in Figure 27.

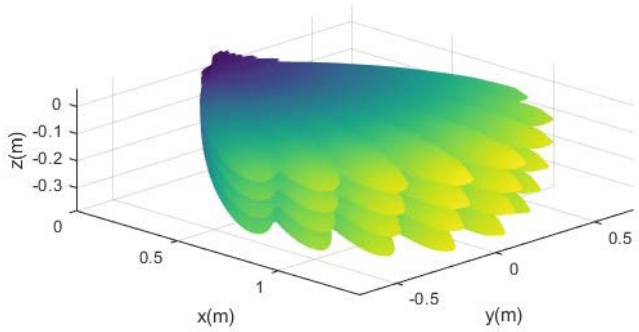

(a) Iso-surface

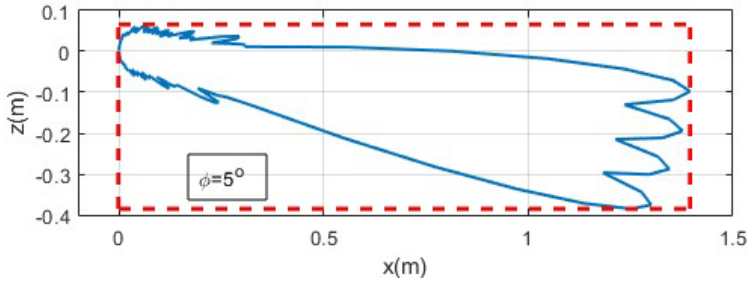

(b) Vertical cut (φ=5°): compliance distance (blue line) and box-shaped compliance boundary (red dashed line)

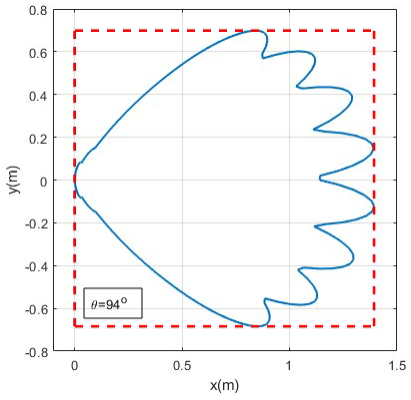

(c) Horizontal cut (ϑ=94°): compliance distance (blue line) and box-shaped compliance boundary (red dashed line)

Figure 27. Compliance boundaries for Nokia AWEUC antenna assuming 1 W transmitted power.

5.8 Logistic sector: Warehouse, 5G FR2

The current exposure scenario is based on a private 5G FR2 base station located in a warehouse in Belgium. Full technical description can be found in D 2.2. The compliance boundaries of the modelled antennas are presented in Figures below (Figure 28 –Figure 32).

a. 2x2 array

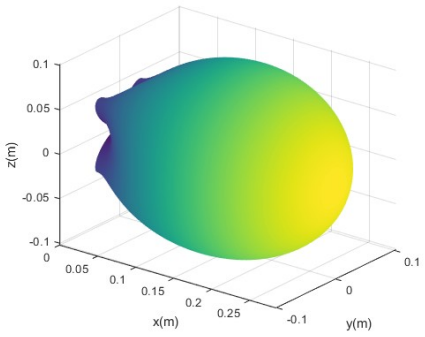

(a) Iso-surface

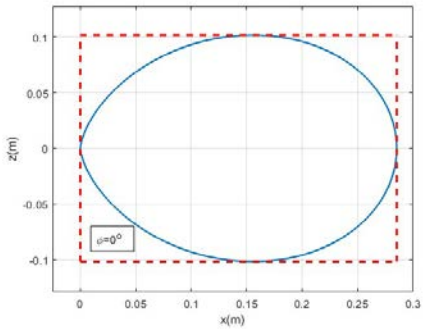

(b) Vertical cut (φ=0°): compliance distance (blue line) and box-shaped compliance boundary (red dashed line)

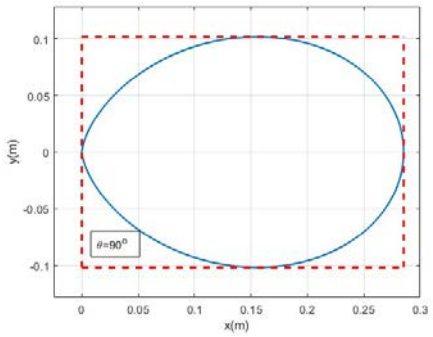

(c) Horizontal cut (ϑ=90°): compliance distance (blue line) and box-shaped compliance boundary (red dashed line)

Figure 28. Compliance boundaries for 2x2 FR2 BS antenna assuming 1 W transmitted power.

b. 4x4 array

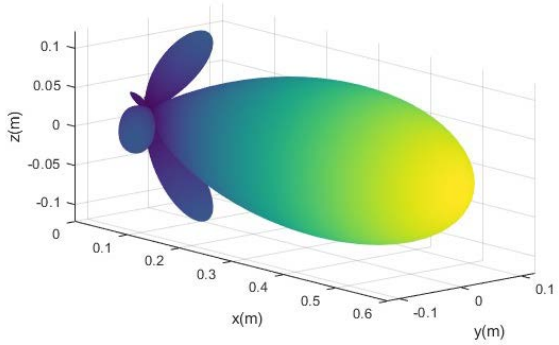

(a) Iso-surface

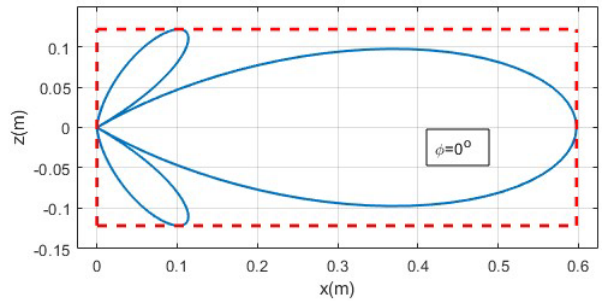

(b) Vertical cut (φ=0°): compliance distance (blue line) and box-shaped compliance boundary (red dashed line)

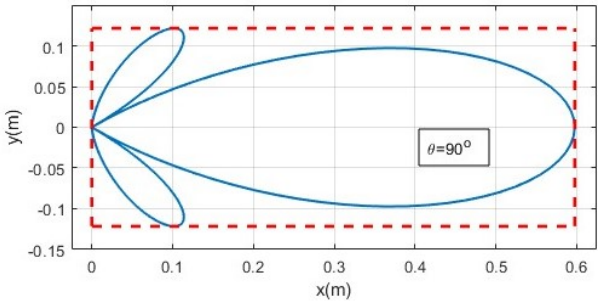

(c) Horizontal cut (ϑ=90°): compliance distance (blue line) and box-shaped compliance boundary (red dashed line)

Figure 29. Compliance boundaries for 4x4 FR2 BS antenna assuming 1 W transmitted power.

c. 6x6 array

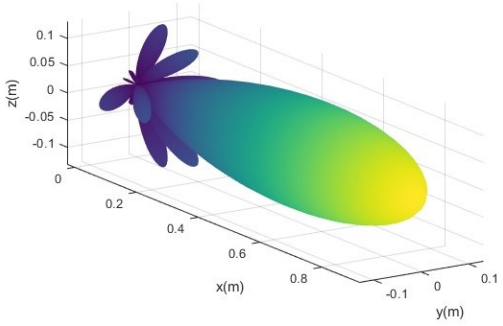

(a) Iso-surface

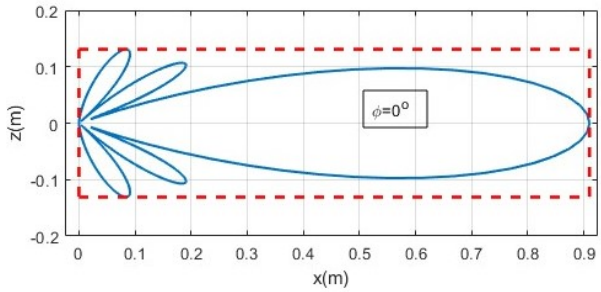

(b) Vertical cut (φ=0°): compliance distance (blue line) and box-shaped compliance boundary (red dashed line)

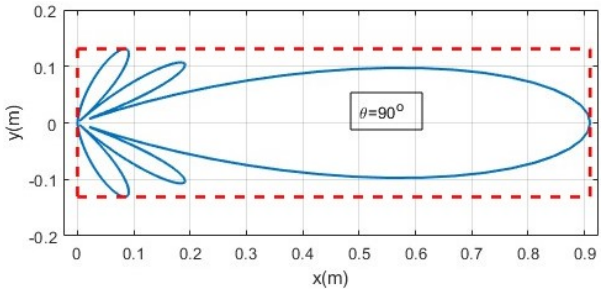

(c) Horizontal cut (ϑ=90°): compliance distance (blue line) and box-shaped compliance boundary (red dashed line)

Figure 30. Compliance boundaries for 6x6 FR2 BS antenna assuming 1 W transmitted power.

d. 8x8 array

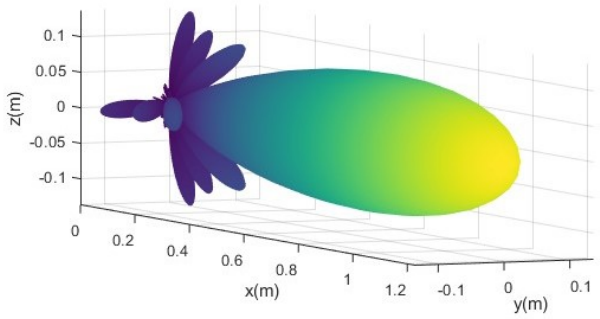

(a) Iso-surface

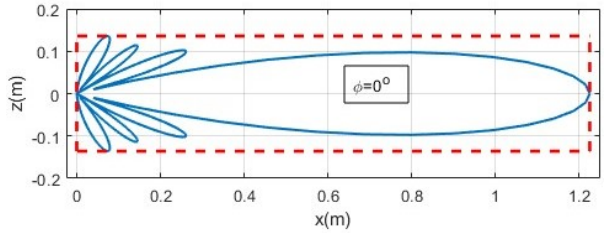

(b) Vertical cut (φ=0°): compliance distance (blue line) and box-shaped compliance boundary (red dashed line)

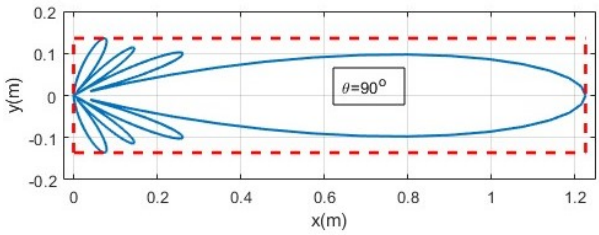

(c) Horizontal cut (ϑ=90°): compliance distance (blue line) and box-shaped compliance boundary (red dashed line)

Figure 31. Compliance boundaries for 8x8 FR2 BS antenna assuming 1 W transmitted power.

e. 10x10 array

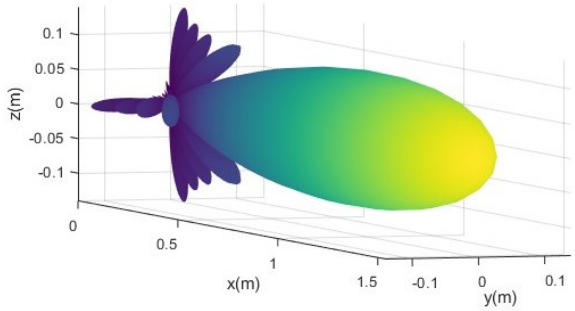

(a) Iso-surface

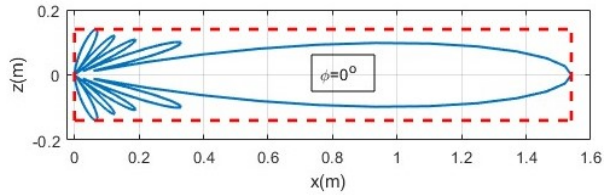

(b) Vertical cut (φ=0°): compliance distance (blue line) and box-shaped compliance boundary (red dashed line)

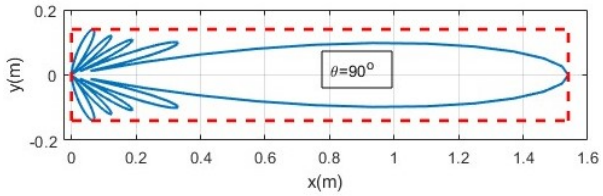

(c) Horizontal cut (ϑ=90°): compliance distance (blue line) and box-shaped compliance boundary (red dashed line)

Figure 32. Compliance boundaries for 12x12 FR2 BS antenna assuming 1 W transmitted power.

6 Limitations for estimating occupational exposure

Despite good results of model validation, it is important to reflect on possible error sources and limitations of the generic model. We identify three sources of errors in the generic model. Some of the below listed errors are valid also for numerical calculations in general.

1. **Human errors** in the inputs: a first source of errors is due to human errors: e.g., reading inputs from a wrong datasheet, entering wrong area size or clutter percentage as model input, mistyping input values...

2. **Simplification errors** on the inputs: as the approach intends to be accessible for laymen, there are inherent errors due to simplification of the inputs: e.g., the antenna pattern can only be approximated as either wall mounted antenna with directivity or ceiling mounter antenna with omnidirectional radiation pattern, the base stations might not all have the same power or height or antenna pattern, the clutter might be heterogeneous in height and material...

3. **Propagation environment errors**: the propagation environment will also be a source of errors. It is itself a simplification of the real configuration: not all material parameters (e.g., permittivity and conductivity) are entirely correct, not all clutter is modeled, temporal variations due to moving humans or machinery are not accounted for... The environment should be very well characterized by an accurate environment model and the model input parameters should be well known and checked for their correctness. Still, some errors are impossible to eliminate. All numerical calculations (and for beamforming antennas also measurements) are subjected to the error in the technical data provided by the manufacturer, mainly antenna radiation patterns. Antenna radiation patterns are determined either by measurements or by numerical calculations, and therefore have uncertainty. Besides, they are determined for coverage reasons, meaning they are accurate in a far field region. For antennas with high directivity, like beamforming antennas, the direction (azimuth and elevation) from the antenna to the point of observation becomes very important. At the edge of the main beam, even such small difference as 1° results in a difference of antenna gain in the range of 10 dB. And even if the environment was perfectly modeled, real values would still deviate from simulations to some extent, due to errors caused by the ray tracing approximation. Alternatively, the model could be built based directly on real experimental data instead of on simulations, which would correctly reflect the real propagation phenomena at play. However, building a model based on measurement data would be a tremendous effort, given the large amounts of data that are required for building such generic machine learning based model. And even the measurement data itself will not be a 100% truthful representation of reality, due to measurement uncertainties.

4. **Generic model errors**:

a) machine learning model performance: even when assuming no errors under points 1, 2 and 3, validation of the generic model showed that the generic model does not have a perfect performance. It will inherently provide an estimation (and hence, an

approximation) of the E-field levels, as is not able to fully mimic the propagation model used in the ray tracing simulation (or predict E data in case of measurement).

b) Limited model applicability: besides the model being an inherent approximation, the model performance is also expected to deteriorate for configurations of which the input parameters lie outside the input space that was covered by the training dataset. E.g., if we have used training data for transmitter densities varying between 1 and 5 transmitters per 1000 m², the model is expected to perform relatively well for a new configuration with a transmitter density of 3.3 transmitters per 1000 m². However, when the constructed model is created for a configuration with a transmitter density of 8 base stations per 1000 m², it is expected to be less accurate. As such, when the model relies on N input parameters, its preferred applicability is within the N-dimensional subspace that is defined by the range of the N input parameters in the training data. This might exclude some new environments from being reliably evaluated or tested.

5. **Duty cycle errors**: our model assumes a worst-case scenario where each of the transmitters is always on (duty cycle 100%). Adding realistic data usage and traffic models to the generic model would allow making more realistic estimates of the real exposure, but it can for now be considered as a worst-case exposure representation. At the moment there are very limited data available regarding the real duty cycles in private networks and especially the amount of uplink data, which greatly affects the average exposures.

6. **Downlink**: our model only accounts for downlink exposure. The amount of existing uplink exposure studies is limited; creating a generic model truthfully representing this would be very challenging: it might involve mobility of transmitting nodes, a large variety of devices (with their specific uplink powers and traffic patterns), a possibly very irregular placement of nodes (compared to base stations which have a logical planning), …

7. **Differences in models**: each numerical tool has its strengths and weaknesses. For example, NARDA model, by including partial transmission, even if uniformly applied, offers more realistic predictions in cluttered zones where some energy penetration through racks is expected. The MATLAB model, on the other hand, is more accurate in modeling material-specific reflections, which gives more precise and detailed contributions of reflections, important especially in high reflective environments with metallic structures. Nevertheless, because both models aligned well with measurements in representative parts of validated scenarios, we consider their predictions reliable also in areas that were not directly validated (unmeasured areas) and to be within a reasonable margin of uncertainty. Importantly, using two independent modeling approaches provides confidence in the robustness of the overall assessment, especially when combined with spatially distributed measurements.

7 RF EMF exposure of workers

7.1 Maximal and mean exposure of workers

The RF EMF exposure of the workers due to a real private 5G networks was analyzed for various scenarios which are described in details in the D 2.2 and D 2.3., respectively.

Analysis of the exposure scenarios of workers detailed in Deliverable 2.2 reveals that the highest radiofrequency exposure levels were associated with macro-outdoor 5G-FR1 base stations. These stations, with transmission powers of up to 100 W, are deployed to provide coverage across extensive outdoor areas, such as those found in logistics centers (e.g., ports). For personnel working within the coverage area of these base stations, the maximum recorded field strengths were an E95 (maximum) value of up to 16.44 V/m and an E50 (median) value of up to 8.29 V/m. Lower, yet notable, exposure was characterized in an indoor research laboratory housing a fully operational standalone (SA) 5G-FR1 base station operating at 20 W for technology testing. In this environment, the measured E95 reached 11.31 V/m, with a median (E50) value of 4.01 V/m.

Significantly lower exposure levels of users[1] were measured in scenarios utilizing low-power 5G-FR2 base stations, which employ mMIMO antenna technology and transmission powers of up to 1 W, typically deployed in industrial and research settings. Here, the maximum E95 for user (worker) did not exceed 6.41 V/m, and the median (E50) was 2.67 V/m. For comparison, user[2] exposure from a Wi-Fi 6 network was also assessed, yielding values comparable to the 5G-FR2 scenario, with a maximum E95 of 3.52 V/m and a median (E50) of 1.51 V/m.

Table 16. Worst case exposures scenarios that can be expected due to operation of private networks.

scenario \ type of result				E [V/m]			/
	system	Frequency (GHz)	power	E95 - 95th percentile	E50- median value	standard deviation	*QDC
Logistic sector: Port, public slice (outdoor)	FR1	3,5	100 W	**16,44**	**8,29**	10,2	0.43
Research labs, test facility	FR1	3,5	20 W	**11,31**	**4,01**	8,01	0.27
Smart Industry 4.0: warehouse - user	FR2	28	1W	**6,41**	**2,67**		
Research labs - user	FR2	26	1W	**7,2**	**2,61**	4,55	0.30
Office - Wi-Fi 6 – user	Wi-Fi	5,5	0.2 W	**3,52**	**1,51**		
Office - Wi-Fi 6 - nonuser	Wi-Fi	5,5	0.2 W	**2,24**	**0,61**		
Smart Industry 4.0: production site	FR1	3,6	1W	**1.14**	**0.74**	0.77	0.30
Smart Industry 4.0: warehouse - nonuser	FR2	28	1W	**0,71**	**0,59**		
Smart Industry 4.0: warehouse	FR1	3,6	1W	**1,06**	**0.34**	0.60	0.43

[1] The direction of the user (worker) was determined by identifying the ray with the lowest path loss. Using the angle of departure of that ray, a steering vector was calculated and applied to the elements of the transmitter's antenna array, resulting in a high-gain beam directed toward the user.

[2] Wi- Fi 6 also employs beamforming to steer the signal to a specific user rather than broadcasting it in all directions.

The lowest recorded exposure levels were characterized for workers (non-users) in Smart Industry 4.0 environments utilizing low-power 5G-FR2 base stations and Wi-Fi 6, which operate at transmission powers of up to 1 W. Similar values were found in smart industry facilities of a key global leader in smart IoT solutions where low-power 5G-FR1 pico indoor remote radio heads (pRRH) served as small cell access points with a maximum power of 1 W. In these settings, the measured field strengths reached a maximum (E95) up to 1.14 V/m, with a median (E50) value up to 0.74 V/m.

Evaluation of RF EMF exposure of workers to different frequency ranges within the smart industry sector reveals distinct characteristics for 5G FR1 and FR2 systems.

For 5G FR1, simulations indicate a considerable variation in exposure levels across different deployment scenarios. The highest median exposure (E50) of 8.29 V/m was identified in the logistics sector, specifically from a macro-cell installation. Conversely, the lowest median exposure of 0.34 V/m was found in an Industry 4.0 warehouse environment utilizing a low-power pico-cell. An intermediate level (E50 = 4.01 V/m) was characterized in an office test facility with a micro-cell. The elevated field strengths in the logistics are attributable to high antenna input powers (up to 100 W), the use of directional antennas, and deployment at lower heights, which collectively reduce path loss. For context, a laboratory Wi-Fi 6 scenario was also modelled, yielding field strengths comparable to the warehouse and production hall environments, with only a marginal exposure increase for active users relative to non-users in the vicinity.

For 5G FR2, exposure patterns are primarily governed by scenario definition and antenna configuration. The research laboratory scenario was assessed using a conservative envelope approach, considering all potential beam directions to determine the maximum possible exposure. In contrast, the Smart Industry 4.0 warehouse scenario employed spatial averaging across predefined user and non-user locations to establish a representative exposure level. Analysis confirms that non-user exposure is largely independent of beamwidth, whereas narrower beams concentrate radiated energy on intended users, substantially increasing their exposure. This disparity is quantified by a reduction in field strength for non-users relative to users, ranging from 69% to 91% for the E95 value and from 32% to 82% for the median (E50) value.

Furthermore, increasing the antenna array size from a 2x2 to a 10x10 configuration was found to amplify user exposure by approximately a factor of five for both E50 and E95 values, a consequence of enhanced directivity and beamforming gain. Conversely, non-user exposure demonstrated only a marginal increase, by factors of approximately 1.25 (E50) and 1.42 (E95), as these locations remain outside the primary beam lobes. A key overall finding is that, despite differing operational frequencies and antenna technologies, the estimated exposure levels for both FR1 and FR2 systems fall within a comparable range.

All analyzed exposure scenarios confirmed that the measured RF-EMF levels remain substantially below the established regulatory limits. The recorded field strengths were well under the action values of 140 V/m stipulated in Directive 2013/35/EU [11] and the reference levels of 61 V/m set by Recommendation 1999/519/EC [10] that are used for workers at particular risks or workers not working with sources of EMF. This substantial margin of compliance ensures a high degree of protection for all workers, including those at particular risk, such as individuals with active or passive implanted medical devices, body-worn medical equipment, and pregnant workers [12].

Numerical simulations, validated by in-situ measurements, indicate that the maximum exposure level (E95) from private 5G networks in an outdoor environment where macro 5G base stations are used (a logistic center at the Port of Koper) is well below established regulatory limits. Specifically, it does not exceed 2% of the action level in Directive 2013/35/EU [11] and 10% of the reference level in Recommendation 1999/519/EC [10].

In a typical indoor industrial environment where pico 5G base stations are deployed (a smart Industry 4.0 production and warehouse facility), the measured exposure was substantially lower. The maximum (E95) and median (E50) values were found to be no more than 0.006% of the action level in Directive 2013/35/EU [11] and 0.03% of the reference level in Recommendation 1999/519/EC [10].

7.2 Temporal and Spatial variability

While band-selective measurements under high traffic loads (e.g., speed tests) or through extrapolation provide worst-case exposure scenarios, the real-time average exposure in private 5G networks is highly dynamic. This temporal variability contrasts sharply with the more static fields of previous generations and is governed by two principal factors:

1 **Speed test:** 5G Base Stations only emit high-power beams when there is active data traffic (downlink/uplink). This means:
   - Average Exposure is much lower than the worst-case maximum (extrapolated) exposure.
   - The maximum-to-median power density ratio for the 5G is notably higher than for older technologies, especially when beamforming is active, reflecting the bursty, dynamic nature of the beams.
   - Averaging Time: Regulatory compliance standards (ICNIRP 2020) account for this by stipulating a time-averaging period (e.g., 6 minutes for frequencies above 6 GHz, and Basic Restrictions for sub-6 GHz). Concerns about worker safety frequently focus on electromagnetic field (EMF) exposure, particularly how exposure varies over time in real industrial operations. Regulatory standards such as the ICNIRP 2020 guidelines and the EU Directive 2013/35/EU require that exposure be evaluated over a 6-minute averaging period for compliance. Measurements show that using a longer averaging time (e.g., 30-min average) significantly reduces the observed variability in E-field measurements, bringing the 5G band variability in line with that of previous generations. This confirms that the short-term high peaks are averaged down for thermal safety compliance.

2 Geometry conditions: there are multiple factors contributing to the average exposures being much lower than worst case exposures.

- During their daily shift workers move around the workplace, meaning even at the worst case situation, where there is a maximum exposure at their most common working position, the average will be lower due to the time spent at other locations.
- There are different fixed obstacles at workplace increasing path loss to the location of the worker.
- There are movable obstacles at workplace that increase path loss to the location of the worker for some specific time intervals.

In essence, workers are exposed to dynamic, high-intensity fields only momentarily—when actively receiving a dedicated mMIMO beam—while both spatial and temporal average exposure levels remain low.

7.2.1 Temporal variability

Temporal in-situ measurements were performed for several exposure scenarios of workers. However, real traffic conditions were largely absent; while the network infrastructure was operational, user traffic was minimal due to lack of operational IoT devices in industry processes. In most cases, controlled speed tests were initiated to generate a measurable signal. The measurement details and results for each scenario are as follows:

1. **Logistics Sector (Port of Koper, Private 5G FR1):** A 6-minute measurement was conducted with the base station operational but idle. A 30-second speed test was performed to simulate load. The maximum instantaneous field strength was 4.78 V/m, while the 6-minute average was 1.16 V/m, indicating that the average exposure was more than 15 times lower than the peak value.

2. **Logistics Sector (Port of Koper, Public Network Slice 5G FR1):** A 60-minute measurement was performed on a public network slice. The maximum instantaneous value was 5.01 V/m. The average exposure values were 0.77 V/m (1-minute), 0.48 V/m (6-minute), and 0.39 V/m (30-minute). The maximum 6-minute average was more than 100 times lower than the instantaneous peak.

3. **Smart Industry 4.0 (Warehouse, Private Standalone 5G FR1):** Over a 45-minute period with minimal traffic, the maximum instantaneous field strength was 0.32 V/m. The average values were 0.09 V/m (1-minute), 0.06 V/m (6-minute), and 0.04 V/m (30-minute). The 6-minute average exposure was 25 times lower than the maximum.

4. **Smart Industry 4.0 (Production Hall, Private Standalone 5G FR1):** A 30-minute measurement under minimal traffic conditions recorded a maximum instantaneous value of 1.19 V/m. The average exposure was 0.25 V/m (1-minute), 0.16 V/m (6-minute), and 0.12 V/m (30-minute). The 6-minute average was a factor of 50 lower than the peak.

5. **Office (Production Site, Private 5G FR1):** During a 20-minute measurement, the network served one surveillance camera, generating primarily uplink traffic. The maximum

instantaneous field strength was 2.55 V/m, with average values of 1.88 V/m (1-minute) and 1.17 V/m (6-minute). The 6-minute average was 4.8 times lower than the maximum.

6. **Research Laboratory (Private Non-Standalone 5G FR2):** In a 10-minute period with an idle base station, a 60-second speed test was conducted. A high maximum instantaneous field strength of 20.95 V/m was recorded. The average exposure was significantly lower: 2.61 V/m (1-minute) and 1.10 V/m (6-minute), making the 6-minute average 360 times lower than the peak.

7. **Terberg terminal tractor, 5G FR1**. Terberg terminal tractor is a case, where the exposure was due to the operation of a 5G modem, integrated in the terminal tractor. There was active video stream running from the Terberg terminal tractor to the network as well as active transfer of live vehicle status and diagnostic data, as it will be used in the future. Measurements were carried at the position of the driver and passenger for a duration of 10 minutes. The maximum measured value in the 10-minute period was 2.60 V/m for drivers and 2.65 V/m for passengers, whereas maximum 1 minute average value was 0.90 V/m for drivers and 0.86 V/m for passengers, and 6-minute average was 0.64 V/m for drivers and 0.58 V/m for passengers. Therefore, maximum 6-minute average exposure was 15 times lower than the maximum value.

While the present findings clearly indicate that temporally averaged exposure values are significantly lower than peak levels, these measurements were conducted under minimal traffic loads. Projecting real-world exposure is challenging due to a lack of data on typical private network usage during the measurement campaigns of the SEAWave project. Such networks are expected to generate substantial uplink traffic from numerous sensors and monitoring devices in the future. Therefore, operational scenarios involving high-density, simultaneous device communication could result in average exposure levels that exceed those recorded here.

The analysis of temporal variability of workers exposure reveals several key points:

- **Low Baseline Exposure**: Workers are typically exposed to EMF levels comparable to or lower than those from Wi-Fi systems in the same facility.
- **Cause of Variability**: Short-duration bursts, which occur when devices transmit data or a worker is briefly near a beamformed communication link, are the primary drivers of exposure variability.
- **Importance of Averaging**: The regulatory 6-minute averaging period is highly effective. Even for shorter spikes due to high rata transmission, the resulting 6-minute average remains subdued. The ratio between maximum value and 6-minute average was usually higher than 10.
- **Significant Safety Margin**: Across all measured and simulated scenarios, worker exposures were consistently 10 to 20 times lower than regulatory limits, and often more than 100 times lower.
- **Practical Implication**: The daily variability in a worker's EMF exposure is modest, predictable, and unequivocally safe under current regulatory frameworks.

7.2.2 Spatial variability

Spatial variability of electric field distribution of private 5G networks has an important contribution to the exposure of the workers. This is becoming even more important with the introduction of beamforming technology due to the ability of the network equipment to steer

the energy only in the direction where there is active need for data transfer. For non-beamfoming networks, spatial variability of the exposure is constant, as radiation patterns of the antenna do not change their properties with time. But with introduction of beamforming, spatial variability of the exposure changes with time depending on the

- usage of the network: position of user equipment, current data transfer, number of devices...;
- on technical parameters of the network, like beamsets in use, position and orientation of antennas, maximum output power...;
- and on many other parameters, like material properties of surrounding objects, position and height of neighboring objects...

Spatial variability was assessed by raster, walk-through and spatial measurements as well as by numerical calculations. For most of measured scenarios, numerical calculations were performed for the whole area of interest. These results are given in chapter 3 Validation of various exposure scenarios. There, for each dataset:

- results of raster measurements,
- values of numerical calculations on the same locations as raster measurements for at least one numerical model and
- values of numerical calculations on all calculated points, usually in a 0.1×0.1 m grid

following data are available that give insight in spatial variability of the electric field:

- 95th, 75th, 50th and 25th percentile, standard deviation and quartile coefficient of dispersion;
- CDF graph,
- figure representing spatial distribution of the calculated electric field as well as results of raster measurements.

Results show that some real exposure scenarios have great spatial variability of electric field values. In Table 17 overview of quartile coefficient of dispersion (QCD) is given, which is a robust measure of dispersion of results. From results we can see that the lowest value of QCD was obtained for Office, test facility of wireless networks, private 5G FR1 scenario and for Smart Industry 4.0: Production Hall, private SA 5G FR1 scenario. There, variability of the field was smaller compared to scenarios with high QCD values, like Logistic sector: Port of Koper, public slice 5G FR1 scenario or Logistic sector: Port of Koper, private 5G FR1. The reasons for these differences are different. For Logistic sector: Port of Koper, public slice 5G FR1 scenario use of beamforming antennas yields to greater spatial variability. For Logistic sector: Port of Koper, private 5G FR1, the reason is antenna height: it was positioned really low, at 1.9 m, therefore close to antenna, there are high values.

Table 17. Overview of quartile coefficient of dispersion (QCD) for different scenarios.

scenario	measurements	result of numerical modeling at					
		same locations as measurement was taken			all calculated points (usualy grid size 0.1×0.1 m)		
		MATLAB 1	MATLAB 2	NARDA	MATLAB 1	MATLAB 2	NARDA
Logistic sector: Port of Koper, private 5G FR1	0.45	0.31	0.32	0.31	0.36	0.36	0.33
Logistic sector: Port of Koper, public slice 5G FR1	0.58			0.25			0.25
Smart Industry 4.0: Warehouse, private SA 5G FR1	0.43	0.74		0.39	0.88		0.38
Smart Industry 4.0: Production hall, private SA 5G FR1	0.30			0.14			0.29
Office, test facility of wireless networks, private 5G FR1	0.21	0.22		0.27	0.49		0.37
Research laboratory, private NSA 5G FR2	0.30		0.36	0.41		0.75	0.89

Walk-through measurements were conducted in Smart Industry 4.0: Warehouse, private SA 5G FR1 and Smart Industry 4.0: Production Hall, private SA 5G FR1 scenarios. Here, measurements were carried along the corridors in both objects. For Smart Industry 4.0: Warehouse, private SA 5G FR1 scenario, the value of the QCD was 0.39, varying from 0.22 in corridor 3 to 0.51 in corridor 4. The E95 value was 1.15 V/m, whereas the E25 value was 0.23 V/m. For Smart Industry 4.0: Production Hall, private SA 5G FR1 scenario, the value of the QCD was 0.32, varying from 0.27 in corridors 3 and 4 to 0.52 in corridor 1. The E95 value was 1.45 V/m, whereas the E25 value was 0.42 V/m.

Spatial measurements were carried out for several exposure scenarios. Measurements followed the IEC 62232:2022 [13] standard scheme for spatial averaging at three heights (1.1 m, 1.5 m, 1.7 m) and three lateral positions (center, 0.2 m left, 0.2 m right), yielding nine measurements. Two additional vertical planes (0.2 m in front and 0.2 m behind) increased the total to 27 measurement points.

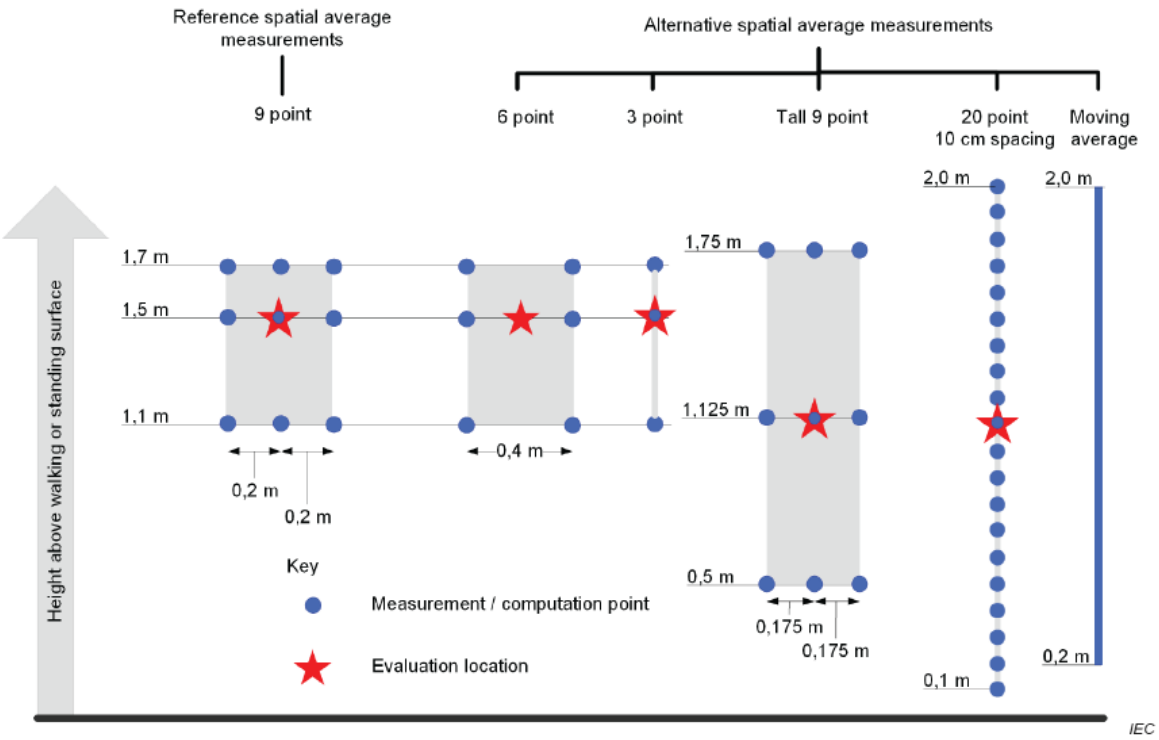

Figure 33. Spatial measurement scheme according to IEC 62232:2022 standard.

Spatial averaging was analyzed for several scenarios. Difference between the reference 9-point average value and one point value at the height of 1.5 m was:

- Logistic sector: Port of Koper, public slice 5G FR1: 2.6%;
- Smart Industry 4.0: Production hall, private SA 5G FR1: -2.8%;
- Office, test facility of wireless networks, private 5G FR1: -22.3%;
- Research laboratory, private NSA 5G FR2: 72.6%.

With the exception of the last results, all other results of spatial averaging show that one point measurement at the height of 1.5 m reliable represents the exposure at the location. The reason for such great difference for the last scenario Research laboratory, private NSA 5G FR2 is the fact that in this scenario antenna was mounted at the height of 1.5 m. Spatial measurements were carried at the distance of 3 m from antenna. There, electric field is still very inhomogeneous due to high directivity of beamforming FR2 antenna. There, averaging really predicts the whole-body exposure better, however by averaging we would lose detailed information about the behavior of the electric field in proximity to beamforming high gain antenna.

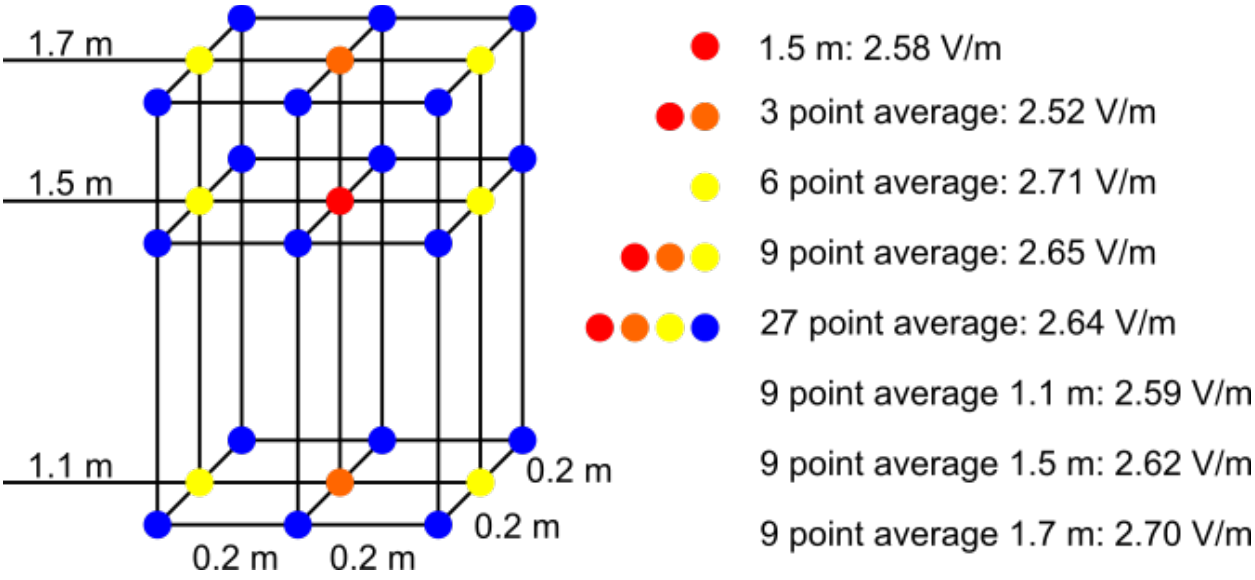

Figure 34. Spatial measurement results for Smart Industry 4.0: Production Hall, private SA 5G FR1 scenario.

Analysis of user versus non-user exposure for FR2 beamforming exposure scenario is given at the beginning of the chapter 8 RF EMF exposure of workers. There, it was found that the exposure of non-users is significantly lower: a reduction in field strength for non-users relative to users, ranging from 69% to 91% for the E95 value and from 32% to 82% for the median (E50) value.

7.2.3 Risk of overexposure

Results show that the exposure on normal workplaces will remain low even after the introduction of private networks in Industry 4.0. However, as shown in chapter 5 Compliance boundaries of emissions from New Local Networks in Industry 4.0. there are zones around typical sources, used for private networks, where both action values of Directive 2013/35/EU [11] and reference levels of Recommendation 1999/519/EC [10] are exceeded. Access to these areas should be permitted only to trained workers, for which risk assessment for EMF exposure has been carried. Nowadays such sources, used for public mobile networks, are usually mounted on towers or poles, where the unwanted accidental overexposure is very unlikely. With the introduction of such sources inside the halls and other working environments the chance of accidental overexposure is increased.

Assuming that the antennas examined are representative of typical installations in work environments and considering a 2 m tall person standing beneath the antenna, a minimum installation height of approximately 2.5 m for indoor antennas and 4.5 m for outdoor antennas ensures compliance with the exposure limits for the general public. For compliance with occupational exposure limits, the installation height can be reduced to approximately 2.2 m and 3.1 m for indoor and outdoor deployments, respectively. For installations at lower heights and indoor antennas, the maximum distance from the antenna of the exclusion zone could extend to over 1.5 m for general public exposure and 70 cm for occupational exposure. For outdoor

antennas, these distances could reach approximately 14 m and 6 m for general public and occupational exposure respectively.

7.2.4 Comparison to other networks deployed in smart Industries

Private 5G networks used in Smart Industries exhibit variable exposure characteristics depending on frequency band and deployment. Sub-6 GHz operations produce exposure profiles broadly comparable to 4G macrocell networks, albeit with potentially higher localized levels near densely deployed low-power small cells offset by reduced per-cell transmit power, while millimeter wave (mmWave) deployments generate highly focused, shallow-penetration (skin-surface level) EMF due to beamforming and obstruction losses, resulting in significantly lower whole-body exposure outside of the beam path. Compared to other industrial systems, typical 5G small cell exposure (0.1–2 W) is analogous to Wi-Fi routers (0.05–0.1 W) or LoRaWAN gateways (0.5–5 W) at similar proximity, although user devices (e.g., smartphones) often dominate personal exposure during active use (0.1–0.5 W peak for 5G/4G vs. 0.01–0.05 W for Wi-Fi). Technologies like LoRa end-devices and Bluetooth exhibit negligible exposure due to ultra-low power (≤0.1 W) and sporadic transmission duty cycles. When compared to Zigbee, 5G exposure will be significantly higher, as Zigbee uses limited transmit powers and focuses on lower data rates, which will low power consumption. Similarly, other industrial wireless technologies like WirelessHART also focus on lower data rates with limited transmit power. Their main use is process monitoring and optimization, while 5G enables more advanced functionalities like robotics, low-latency video streaming, etc. Generally speaking, all systems operate well below international exposure guidelines and EU directive for workers, with worker exposures typically representing 0.01–0.1% of permissible levels.

8 Conclusion

The validation results demonstrate that both the detailed numerical models and the developed generic model are capable of providing reliable estimates of electromagnetic field exposure in realistic environments. The numerical tools showed very good agreement with measurements, particularly in the assessment of typical and high-end exposure levels, with discrepancies primarily arising from geometric and antenna modeling limitations or uncertainties in measurement positioning. When sufficient detail is included in the modeling of the environment and sources, these tools can accurately predict the electric field even at specific locations.

The generic model also showed strong agreement with both measured and simulated data, successfully reproducing the median and 95th percentile of the electric field values in most scenarios within the uncertainty estimated from the measurement dataset. Deviations were observed mainly in cases where input parameters, such as the antenna directivity, lay outside the range used for model training. These results confirm that the generic model provides an easy and computationally efficient alternative for estimating EMF exposure in occupational environments, while its performance can be further enhanced by expanding the training dataset to include a broader variety of configurations.

Overall, the combined validation efforts confirm that both the numerical and generic modeling approaches are effective tools for exposure assessment, offering complementary strengths: the numerical models provide high accuracy for detailed analyses, while the generic model can be used for rapid exposure estimation across diverse scenarios.

In addition to the “in situ” measurements, numerical modeling with two different tools was used to estimate the electric field distribution in the warehouse and the production hall. Both models demonstrated relatively good overall agreement with the measured values, particularly in terms of maximum, average, and 95th percentile levels, with differences generally below 20%. Although local deviations occurred due to the complex and inhomogeneous nature of pallet rack loading and limited information on material properties, the models provided valuable spatial insight and were shown to be effective for estimating exposure levels in areas not directly measured. Importantly, numerical modeling can also help identify potential exposure hotspots that might be overlooked during spot measurements, especially in large or cluttered environments. These results support the use of numerical modeling as a complementary method to measurements, particularly for RF EMF exposure assessment of indoor private 5G networks installed in large spaces.

The RF EMF exposure of workers due to private standalone (SA) 5G networks in various scenarios in a smart industry facility was found to be very low and far below the current exposure limits for workers. It is expected that this could be similar to most indoor scenarios in smart industry sectors where pico indoor remote radio heads (pRRH) are enrolled due to the relative low output power of base stations used for indoor private networks. Using multiple low-power pRRHs benefits from the ability to obtain good coverage in various indoor scenarios, even in an

environment with a lot of clutter. It is also a common practice to mount the pRRH at ceiling level, mainly to obtain good coverage, thus reducing exposure at worker-accessible locations. In the studied case, the pRRHs were located just under the roof. To minimize the average downlink exposure levels, it is advised to strive for a maximally homogeneous distribution of (lower) electric field levels. This can be realized by either increasing the installation height of pRRHs and increasing their power as needed, or, alternatively, reducing their output power but increasing the number of transmitters accordingly to maintain coverage.

During the measurement process in real factory environment, one location was identified where the pRRH was installed at a lower height of 3.1 m, which represents the worst-case conditions. The maximum electric field value at a sensor height of 1.5 m was 3.1 V/m for measurements and 2.7 V/m for calculations, obtained right below the pRRHs. The 95th percentile value was slightly lower at 2.5 V/m and 2.3 V/m, respectively.

In a typical indoor industrial environment where pico 5G base stations are deployed (a smart Industry 4.0 production and warehouse facility), the measured exposure was substantially lower. The maximum (E95) and median (E50) values were found to be no more than 0.006% of the action value in Directive 2013/35/EU [11] and 0.03% of the reference level in Recommendation 1999/519/EC [10].

Although this study offers a detailed evaluation of worker exposure to RF EMF in an operational smart industry environment, the findings are derived from measurements and simulations performed at a limited numbers of potential variability of implementation of private networks in smart Industry 4.0. Consequently, extrapolating these results to other industrial sectors and settings requires careful consideration [15]. Exposure levels may differ due to factors like variations in transmitter power, deployment density, beamforming antenna configurations, structural design, material composition, and the arrangement of equipment and reflective surfaces. For instance, facilities with higher-power transmitters, antennas mounted at lower heights, or more densely packed metallic infrastructure could exhibit distinct exposure distributions. However, the methodology—combining measurements with numerical modeling—can be applied to other industrial settings for assessing worker exposure.

Emerging technologies promise to revolutionize EMF analysis. Machine learning algorithms trained on vast datasets of simulations and measurements could predict fields in novel scenarios, reducing computational burdens. The synergy of computational modeling and empirical measurement forms the cornerstone of reliable EMF analysis. By rigorously validating simulations against real-world data, engineers and researchers ensure the safety, efficiency, and regulatory compliance of electromagnetic systems. As technology advances, the integration of AI, high-precision sensors, and spatial analytics will further enhance our ability to navigate the invisible landscape of electromagnetic fields.

9 Appendix

9.1 List of abbreviations

ABBREVIATION	MEANING
3G	Third generation of broadband cellular network technology
3GPP	3rd Generation Partnership Project
4G	Fourth generation of broadband cellular network technology
5G	Fifth generation of broadband cellular network technology
5G NR	5G New Radio
5GAA	5G Automotive Association
5G-ACIA	5G Alliance for Connected Industries and Automation
AGV	Automated Guided Vehicles
AMR	Autonomous Mobile Robot
AMR	Autonomous Mobile Robots
APN	Access Point Name
BSS	Basic Service Set
dBi	Antenna gain in decibels relatively to isotropic antenna
DSS	Dynamic Spectrum Sharing
eDRX	Extended Discontinuous Reception
EIRP	Equivalent Isotropically Radiated Power
eMBB	Enhanced Mobile Broadband
eNB	Evolved Node B
eNodeB	Evolved Node B in 4G radio
EPC	Evolved Packet Core
ETSI	European Telecommunications Standards Institute
FR1	Frequency Range 1
FR2	Frequency Range 2
gNB	Next Generation Node B
gNodeB	Next Generation Node B
GSA	Global mobile Suppliers Association
ICT	Information and Communications Technology
LAN	Local Area Network
LTE	Long Term Evolution Technology
LTE-A	LTE–Advanced
LTE-A Pro	LTE-Advanced Pro
LTE-M	Long Term Evolution for Machines
M2M	Machine to Machine
MIMO	Multiple-Input Multiple-Output
MMS	Multi Media Service
mMTC	Massive Machine Type Communications
mmWave	millimeter wave
mTRP	Multiple Transmission and Reception Point
MU-MIMO	MU-MIMO
NB-IoT	Narrow Band IoT
NSA	Non-Standalone
OBSS	Overlapping Basic Service Sets
OFDM	Orthogonal Frequency Division Multiplexing
OFDMA	Orthogonal Frequency Division Multiple Access
OT	Operational Technology
pLTE	Private LTE Network
PSM	Power Saving Mode
QAM	Quadrature Amplitude Modulation
RAN	Radio Access Network
RF	Radio Frequency
SA	Standalone
SMS	Short Messaging Service
SNR	Signal to Noise ratio
TCO	total cost of ownership
TDD	Time Division Duplex
UE	User Equipment
URLLC	Ultra Reliable Low Latency Communications
VoLTE	Voice over LTE
VPN	Virtual Private Network

10 References

1 Shikhantsov, S.; Thielens, A.; Vermeeren, G.; Demeester, P.; Martens, L.; Torfs, G.; Joseph, W. Massive MIMO Propagation Modeling with User-Induced Coupling Effects Using Ray-Tracing and FDTD. IEEE J. Sel. Areas Commun. 2020, 38, 1955–1963.

2 Salem, M.A.; Lim, H.S.; Chua, M.Y.; Chien, S.F.; Zarakovitis, C.C.; Ng, C.Y.; Rahman, N.Z.A. Investigation of EMF Exposure Level for Uplink and Downlink of 5G Network Using Ray Tracing Approach. Int. J. Technol. 2022, 13, 1298–1307.

3 Shikhantsov, S., Thielens, A., Vermeeren, G., Martens, L., Demeester, P., Joseph, W. User and non-user RF-EMF exposure to the downlink Zero-Forcing transmission of distributed Massive MIMO in an industrial environment. The 1st Annual Meeting of BioEM Abstract Book Collection June 19, 2022 - June 24, 2022 Aichi Industry and Labor Center (WINC AICHI), Nagoya, Japan, 405–410.

4 Törnevik, C.; Colombi, D. Accurately Assessing Exposure to Radio Frequency Electromagnetic Fields from 5G Networks. Ericsson White Paper GFTL-21:000987 2021. Available online: https://www.ericsson.com/495136/assets/local/reports-papers/white-papers/5g-and-emf.pdf.

5 Aerts, S.; Deprez, K.; Verloock, L.; Olsen, R.G.; Martens, L.; Tran, P.; Joseph, W. RF-EMF exposure near 5G NR small cells. Sensors 2023, 23, 3145. https://doi.org/10.3390/s23063145.

6 Aerts, S.; Deprez, K.; Colombi, D.; Van den Bossche, M.; Verloock, L.; Martens, L.; Törnevik, C.; Joseph, W. In-Situ Assessment of 5G NR Massive MIMO Base Station Exposure in a Commercial Network in Bern, Switzerland. Appl. Sci. 2021, 11, 3592. https://doi.org/10.3390/app11083592.

7 International Organization for Standardization. 2018. ISO/TS 10974: Assessment of the safety of magnetic resonance imaging for patients with an active implantable medical device.

8 International Organization for Standardization. 2022. ISO 13528. Statistical methods for use in proficiency testing by interlaboratory comparison.

9 https://www.itl.nist.gov/div898/handbook/eda/section3/bootplot.htm

10 The Council of The European Union. (1999). COUNCIL RECOMMENDATION of 12 July 1999 on the limitation of exposure of the general public to electromagnetic fields (0 Hz to 300 GHz) (1999/519/EC). Official Journal of the European Communities, L199, 59–70.

11 The European Parliament and The Council of the European Union. (2013). Directive 2013/35/EU of The European Parliament and of the Council of 26 June 2013 on the minimum health and safety requirements regarding the exposure of workers to the risks arising from physical agents (electromagnetic fields) (20th individual Directive within the meaning of Article 16(1) of Directive 89/391/EEC) and repealing Directive 2004/40/EC. Official Journal of the European Union, L 179/1-L 179/21.

12 European Commission: Directorate-General for Employment, Social Affairs and Inclusion, Non-binding guide to good practice for implementing Directive 2013/35/EU Electromagnetic Fields. Volume 1, Practical guide, Publications Office, 2015, https://data.europa.eu/doi/10.2767/961464

13 IEC. IEC 62232 Determination of RF Field Strength, Power Density and SAR in the Vicinity of Radiocommunication Base Stations for the Purpose of Evaluating Human Exposure; International Electrotechnical Commission (IEC): PO Box 131, CH-1211 Geneva 20, Switzerland, 2022.

14 ICNIRP. Guidelines for limiting exposure to electromagnetic fields (100 kHz to 300 GHz). Health Phys 118(5):483-524; 2020

15 Gajšek, P.; Apostolidis, C.; Plets, D.; Samaras, T.; Valič, B. EMF Exposure of Workers Due to 5G Private Networks in Smart Industries. Electronics 2025, 14, 2662. https://doi.org/10.3390/electronics14132662